Published in final edited form as:
Nature. 2008 March 6; 452(7183): 93–97. doi:10.1038/nature06612.

Identification of a Novel Serotonin/Glutamate Receptor Complex Implicated in Psychosis

Javier González-Maeso[1,2], **Rosalind Ang**[1], **Tony Yuen**[1], **Pokman Chan**[1], **Noelia V. Weisstaub**[5,6], **Juan F. López-Giménez**[8], **Mingming Zhou**[5], **Yuuya Okawa**[1], **Luis F. Callado**[9,10], **Graeme Milligan**[8], **Jay A. Gingrich**[5,6,7], **Marta Filizola**[4], **J. Javier Meana**[9,10], and **Stuart C. Sealfon**[1,3]

[1]Department of Neurology, Mount Sinai School of Medicine, New York, NY 10029. USA.

[2]Department of Psychiatry, Mount Sinai School of Medicine, New York, NY 10029. USA.

[3]Department of Center for Translational Systems Biology, Mount Sinai School of Medicine, New York, NY 10029. USA.

[4]Department of Structural and Chemical Biology. Mount Sinai School of Medicine, New York, NY 10029. USA.

[5]Department of Psychiatry, Columbia University, and the New York State Psychiatric Institute, New York, NY 10032. USA.

[6]Department of Sackler Institute Laboratories, Columbia University, and the New York State Psychiatric Institute, New York, NY 10032. USA.

[7]Department of Lieber Center for Schizophrenia Research. Columbia University, and the New York State Psychiatric Institute, New York, NY 10032. USA.

[8]Division of Biochemistry and Molecular Biology. Institute of Biomedical and Life Sciences. University of Glasgow, Glasgow G12 8QQ. United Kingdom.

[9]CIBER of Mental Health, University of the Basque Country. E-48940 Leioa, Bizkaia, Spain.

[10]Department of Pharmacology. University of the Basque Country. E-48940 Leioa, Bizkaia, Spain.

Abstract

The psychosis associated with schizophrenia is characterized by alterations in sensory processing and perception[1,2]. Some antipsychotic drugs were identified by their high affinity for serotonin 5-HT_{2A} receptors (2AR)[3,4]. Drugs that interact with metabotropic glutamate receptors (mGluR) also show potential for the treatment of schizophrenia[5-7]. The effects of hallucinogenic drugs, such as psilocybin and lysergic acid diethylamide (LSD), require the 2AR[8-10] and resemble some of the core symptoms of schizophrenia[10-12]. Here we show that the mGluR2 interacts via specific transmembrane helix domains with the 2AR, a member of an unrelated G protein-coupled receptor (GPCR) family, to form functional complexes in brain cortex. The 2AR/mGluR2 complex triggers unique cellular responses when targeted by hallucinogenic drugs, and activation of mGluR2 abolishes hallucinogen specific signalling and behavioural responses. In *postmortem* human brain from untreated schizophrenic subjects, the 2AR is up-regulated and the mGluR2 is down-regulated, a pattern that could predispose to psychosis. These regulatory changes suggest that the 2AR/mGluR2 complex may be involved in the altered cortical processes of schizophrenia, and represents a promising new target for the treatment of psychosis.

Correspondence and requests for materials should be addressed to: J.G.M (e-mail: Javier.Maeso@mssm.edu) S.C.S. (e-mail: Stuart.Sealfon@mssm.edu).

The 2AR and mGluR2/3 show an overlapping distribution in brain cortex in autoradiography studies[13]. The mGluR2 and mGluR3 are not distinguished by autoradiographic ligands. We used fluorescent *in situ* hybridization (FISH) to determine whether either of these receptor subtypes are co-expressed by the same neurons. In layer V mouse somatosensory cortex (SCx), *2AR* mRNA positive cells were mostly *mGluR2* mRNA positive. The level of expression in SCx was much lower for *mGluR3* mRNA, which rarely co-localized with *2AR* mRNA (Fig. 1a). Control studies validated assay sensitivity and specificity, and similar 2AR/mGluR2 mRNA co-localization was found in cortical primary cultures (Figs. 1a,b,c, and Supplementary Fig. S1). Translation of 2AR protein in cortical pyramidal neurons was found to be necessary for normal mGluR2 expression. Mice with globally disrupted 2AR expression (*htr2A*−/− mice) showed reduced cortical mGluR2 binding and expression, while mice in which 2AR expression was selectively restored in cortical pyramidal neurons[8,14] showed control expression levels (Supplementary Table S1, and Supplementary Fig. S2). The effects of mGluR2/3 activation on 2AR responses have been generally attributed to synaptic mechanisms[5,6,13,15]. However, the co-localization of *2AR* and *mGluR2* and the reduction of mGluR2 expression levels in *htr2A*−/− mice motivated us to examine whether a direct mechanism contributed to cortical crosstalk between these two receptor systems.

Recent studies have demonstrated that some GPCRs belonging to the same sequence classes can form dimers[16] or, potentially, higher-order oligomers[17]. Although the 2AR and mGluR2 belong to different GPCR classes, we established the existence of 2AR/mGluR2 heterocomplexes by several methods: co-immunoprecipitation of human brain cortex samples (Fig. 1d) and of HEK293 cells transfected with epitope-tagged receptors (Fig. 2b), bioluminescence resonance energy transfer (BRET) (Fig. 1e, and Supplementary Fig. S3), and fluorescence resonance energy transfer (FRET) (Fig. 2d) studies in transfected cells.

To determine whether the formation of the 2AR/mGluR2 complex has functional consequences, we first examined the effects in mouse SCx membranes of an mGluR2/3 agonist on the competition binding of several hallucinogenic 2AR agonists (Fig. 1f, top) and of a 2AR agonist on the competition binding of several mGluR2/3 agonists (Fig. 1f, bottom). The agonist affinities for the 2AR and mGluR2/3 were decreased when receptor/G protein complexes were uncoupled by GTPγS (Supplementary Fig. S4, and Supplementary Tables S2 and S3). Notably, the glutamate agonist LY379268 (LY379) increased the affinity of all three hallucinogens studied for the 2AR binding site. Furthermore, the 2AR agonist DOI decreased the affinity of the three mGluR2/3 agonists for the glutamate receptor binding site. The allosteric interactions observed were eliminated by antagonist for each modulator (see Supplementary Tables S2 and S3 and Supplementary Fig. S4 for additional concentrations of DOI and LY379, and elimination of the allosteric effects by antagonists). Although the glutamate agonists studied do not distinguish between the mGluR2 and mGluR3 subtypes[18], the rarity of *mGluR3* and *2AR* mRNA co-expression in cortex, the absence of evidence for 2AR/mGluR3 complex formation by co-immunoprecipitation, BRET and FRET, and the detection of 2AR/mGluR2 complexes by these same assays, suggest that the crosstalk identified results from 2AR/mGluR2 complexes.

The differences in the capacity of the mGluR2 and mGluR3 to interact with the 2AR and their close sequence similarity provided the basis to identify the specific mGluR2 domains responsible for heterocomplex formation. Study of a series of molecular chimeras of the mGluR2 and mGluR3 (see Fig. 2a) demonstrated that the segment containing transmembrane (TM) helices 4 and 5 of the mGluR2 receptor was both necessary and sufficient for complex formation with the 2AR. The mGluR3 receptor chimera containing only this segment from the mGluR2 (mGluR3ΔTM4,5) was capable of co-immunoprecipitating with the 2AR (Fig 2b), mediating allosteric crosstalk (Fig. 2c) and maintaining close proximity with the 2AR as

indicated by FRET (Fig. 2d). In contrast, mGluR2ΔTM4,5 did not show evidence of complex formation with the 2AR (Fig. 2, Supplementary Figs. S5, S6, and Supplementary Tables S4 and S5 for complete curves, analysis and evidence of membrane expression of all chimeras). The absolute and relative levels of expression of heterologous constructs were comparable to the physiological levels found in mouse SCx, and in cortical primary cultures (Supplementary Fig. S5 and Supplementary Table S4). Our data do not exclude the possibility that the predicted 2AR/mGluR2 heterodimer, a model of which is shown in Fig. 2f, assembles into tetramers or larger receptor oligomers[19,20].

The changes in high affinity binding caused by 2AR/mGluR2 crosstalk suggested that this complex may serve to integrate serotonin and glutamate signalling and modulate G protein coupling[21,22]. This hypothesis was tested by measuring 2AR regulation of $G\alpha_{q/11}$ and $G\alpha_{i}$ proteins. High-affinity activation of $G\alpha_{q/11}$ by the 2AR was reduced by co-expression of mGluR2 (Fig. 2e, and Supplementary Table S6). Interestingly, the activation of $G\alpha_{i}$ by the 2AR was markedly enhanced by mGluR2 co-expression (Fig. 2e, and Supplementary Table S7). The mGluR2-dependent effects on both $G\alpha_{q/11}$ and $G\alpha_{i}$ regulation by the 2AR were reversed in the presence of mGluR2 agonist (Fig. 2e, and Supplementary Tables S6 and S7). Consonant with the co-immunoprecipitation, allosteric modulation and FRET results, the functional assays of G protein activity also show that the TM4−5 segment of the mGluR2, when substituted into the mGluR3, was sufficient for signalling crosstalk to occur (Fig. 2e). These data support the presence of functional and physiological 2AR/mGluR2 complexes that integrate serotonin and glutamate neurotransmission to specify the pattern of G protein regulation.

Similar evidence for specification of G protein subtype regulation was also observed by the endogenous brain 2AR/mGluR2 complex with membranes from cortical primary cultures (Fig 3a). The pattern of G protein regulation in cortical pyramidal neurons has been shown to predict specific behavioural responses to 2AR agonists. Hallucinogenic drugs and non-hallucinogenic drugs activate the same population of 2ARs in cortical pyramidal neurons, but differ in the 2AR-dependent pattern of G protein regulation and gene induction they elicit[8,9]. In brain cortical neurons, the signalling elicited by hallucinogenic and non-hallucinogenic 2AR agonists causes induction of *c-fos* and requires $G_{q/11}$-dependent phospholipase C activation. However, the signalling of hallucinogens such as DOI and LSD acting at the 2AR also induces *egr-2*, which is $G_{i/o}$-dependent. Thus *c-fos* expression results from any 2AR-signalling, and *egr-2* induction is a specific marker for hallucinogen signalling via the 2AR[8,9]. The finding that mGluR2 modulates the G_{i} protein coupling of the 2AR (Fig. 3a, and Supplementary Tables S6 and S7) suggested that this complex might be important for hallucinogen signalling. The induction of *c-fos* by hallucinogenic 2AR agonists or by structurally similar non-hallucinogenic 2AR agonists *in vivo* in mouse SCx and in cortical primary cultures (Fig. 3b, and Supplementary Figs. S8, S9 and S10) was not affected by the mGluR2/3 agonist LY379. In contrast, the hallucinogen-specific induction of *egr-2* was selectively blocked by LY379 in both mouse cortex *in vivo* and in primary cortical cultures (Fig. 3b, and Supplementary Figs. S8, S9 and S10 for FISH results with LSD treatment, and real-time PCR gene assay results with DOI, DOM, DOB, LSD, lisuride and ergotamine). We also studied the effects of LY379 on the head-twitch response (HTR) behavior, which is hallucinogen-specific[8,9]. Similar to its effects on G protein activation and gene induction, the glutamate agonist LY379 suppressed the induction of the HTR by either DOI or LSD (Supplementary Fig. S11). These results suggest that LY379 acts at the 2AR/mGluR2 complex to reduce the hallucinogen-specific $G_{i/o}$ protein signalling and behaviour. To further establish the functional relevance of 2AR/mGluR2 crosstalk, we compared the responses to the mGluR2/3 antagonist LY341494 in *htr2A*+/+ and *htr2A*−/− mice. The locomotor and vertical activities elicited by LY341495 were significantly attenuated in the *htr2A*−/− mice (Fig. 3c), supporting the functional relevance of the 2AR/mGluR2 complex *in vivo* and suggesting that it also influences the endogenous response to glutamate.

The findings that $G_{i/o}$ protein regulation, which is necessary for the effects of hallucinogens[8], is enhanced by the formation of the 2AR/mGluR2 complex and that activation of the mGluR2 component suppresses hallucinogen-specific signalling implicate this complex in the effects of hallucinogens. The neuropsychological effects of hallucinogenic drugs present commonalities with the psychosis of schizophrenia, and both conditions are accompanied by disruptions of cortical sensory processing[10,11,23-27]. We investigated whether the components of the 2AR/mGluR2 signalling complex are dysregulated in brain cortex of subjects with schizophrenia. We determined the density of 2AR and mGluR2/3 binding sites in cortex from schizophrenic subjects and controls who were matched by gender, age, and postmortem delay (Supplementary Tables S8 and S9). The receptor densities in cortical membranes from untreated schizophrenic subjects were significantly altered, showing increased 2AR and reduced mGluR2/3 receptor levels (Fig. 4a, b). mRNA assays showed that expression of *mGluR2* but not *mGluR3* was reduced in schizophrenia cortex (Fig. 4e). The studies in mouse show that activation of the mGluR2 component of the 2AR/mGluR2 complex eliminates the hallucinogen-specific component of the signalling responses to LSD-like drugs. Thus the increased 2AR and decreased mGluR2 found in the brain in schizophrenia may predispose to a hallucinogenic pattern of signalling.

Many laboratories have attempted to determine the density of 2AR in *postmortem* brain from subjects with schizophrenia, and some studies have reported decreased or unchanged 2AR densities[28]. To try to understand the basis for these discrepancies from our results, we first studied the effects of chronic antipsychotic treatment on the 2AR and mGluR2 in mouse. The chronic atypical antipsychotic clozapine specifically down-regulated the level of expression of 2AR and of mGluR2 in mouse SCx (Supplementary Fig. S12). The down-regulation of mGluR2 by clozapine required expression of the 2AR, as it did not occur in *htr2A*−/− mice (Supplementary Fig. S12), and was not induced by the chronic typical antipsychotic haloperidol (Supplementary Fig. S13). In concordance with the effects of clozapine in murine models, the density of 2AR was reduced to control levels in postmortem human brain cortex of schizophrenics treated with atypical antipsychotic drugs (Fig. 4c), and the mGluR2/3 binding sites were also down-regulated (Fig. 4d). The onset of psychosis in schizophrenia usually occurs in later adolescence or early adulthood[1]. We studied the relationship of receptor densities with aging and both [^{3}H]ketanserin and [^{3}H]LY341495 binding displayed a highly significant negative correlation with age (Supplementary Fig. S14). Hallucinations and delusions typically attenuate with aging[29], which correlates with the lower density of the components of the 2AR/mGluR2 complex that we observed in older subjects. Consequently, the marked dysregulation of both 2AR and mGluR2 expression in schizophrenia would be unlikely to be observed in samples from heterogeneous groups including treated patients[28] or in studies including older patients[28,30].

These studies identify the 2AR/mGluR2 complex as a possible site of action of hallucinogenic drugs. The glutamate and serotonin systems have both been implicated in psychotic disorders, and the components of this complex are found to be differentially regulated in cortex from individuals with schizophrenia. The results are consistent with the hypothesis that the 2AR/mGluR2 complex integrates serotonin and glutamate signalling to regulate the sensory gating functions of the cortex, a process that is disrupted in psychosis.

METHODS

A detailed Methods section is available in Supplementary Information. Briefly, all reagents were purchased from commercial vendors except for LY379268 (Eli Lilly and Company). Mouse lines, treatment protocols, behavioural studies, dissections, and primary neuronal cultures, approved by Institutional Use and Care Committees, have been previously described[8,9]. Protocols used for FISH[8], binding assays[8], real-time PCR[8], FRET[17] and co-

immunoprecipitation[17] were performed as previously described or with minor modifications. Epitope tagged, BRET^2, FRET and chimera receptor constructs were generated using standard cloning techniques and were confirmed by sequencing. BRET^2 using *Renilla* luciferase and Green Fluorescent Protein (GFP^2) was performed in HEK293 cells. Matched schizophrenia and control human brains were obtained from autopsies performed in the Basque Institute of Legal Medicine, Bilbao, Spain in compliance with policies of research and ethical review boards for postmortem brain studies.

Supplementary Material

Refer to Web version on PubMed Central for supplementary material.

Acknowledgements

The authors would like to thank Lakshmi Devi and Lidija Ivic for critiquing the manuscript, Susan Morgello and the Manhattan HIV Brain Bank for providing control brain cortex, Itxazne Rodil, Leyre Urigüen and Bernard Lin for assistance with biochemical assays, and the Mount Sinai Microscopy and Microarray, Real-Time PCR and Bioinformatics Shared Research Facilities. We thank the staff members of the Basque Institute of Legal Medicine for their cooperation in the study. We thank James H. Prather of Eli Lilly and Company for a generous gift of LY379268, and Jean-Philippe Pin for graciously providing the signalling peptide sequence of rat mGluR5. This study was supported by the National Institutes of Health, UPV/EHU and Basque Government, Spanish Ministry of Health, REM-TAP Network, the Whitehall Foundation, the Gatsby Foundation, and the American Foundation for Suicide Prevention.

References

1. Freedman R. Schizophrenia. N Engl J Med 2003;349:1738–49. [PubMed: 14585943]
2. Sawa A, Snyder SH. Schizophrenia: diverse approaches to a complex disease. Science 2002;296:692–5. [PubMed: 11976442]
3. Lieberman JA, et al. Serotonergic basis of antipsychotic drug effects in schizophrenia. Biol Psychiatry 1998;44:1099–117. [PubMed: 9836014]
4. Miyamoto S, Duncan GE, Marx CE, Lieberman JA. Treatments for schizophrenia: a critical review of pharmacology and mechanisms of action of antipsychotic drugs. Mol Psychiatry 2005;10:79–104. [PubMed: 15289815]
5. Aghajanian GK, Marek GJ. Serotonin model of schizophrenia: emerging role of glutamate mechanisms. Brain Res Brain Res Rev 2000;31:302–12. [PubMed: 10719157]
6. Marek GJ. Metabotropic glutamate 2/3 receptors as drug targets. Curr Opin Pharmacol 2004;4:18–22. [PubMed: 15018834]
7. Patil ST, et al. Activation of mGlu2/3 receptors as a new approach to treat schizophrenia: a randomized Phase 2 clinical trial. Nat Med 2007;13:1102–1107. [PubMed: 17767166]
8. Gonzalez-Maeso J, et al. Hallucinogens Recruit Specific Cortical 5-HT(2A) Receptor-Mediated Signaling Pathways to Affect Behavior. Neuron 2007;53:439–52. [PubMed: 17270739]
9. Gonzalez-Maeso J, et al. Transcriptome fingerprints distinguish hallucinogenic and nonhallucinogenic 5-hydroxytryptamine 2A receptor agonist effects in mouse somatosensory cortex. J Neurosci 2003;23:8836–43. [PubMed: 14523084]
10. Vollenweider FX, Vollenweider-Scherpenhuyzen MF, Babler A, Vogel H, Hell D. Psilocybin induces schizophrenia-like psychosis in humans via a serotonin-2 agonist action. Neuroreport 1998;9:3897–902. [PubMed: 9875725]
11. Gouzoulis-Mayfrank E, et al. Psychological effects of (S)-ketamine and N,N-dimethyltryptamine (DMT): a double-blind, cross-over study in healthy volunteers. Pharmacopsychiatry 2005;38:301–11. [PubMed: 16342002]
12. Colpaert FC. Discovering risperidone: the LSD model of psychopathology. Nat Rev Drug Discov 2003;2:315–20. [PubMed: 12669030]
13. Marek GJ, Wright RA, Schoepp DD, Monn JA, Aghajanian GK. Physiological antagonism between 5-hydroxytryptamine(2A) and group II metabotropic glutamate receptors in prefrontal cortex. J Pharmacol Exp Ther 2000;292:76–87. [PubMed: 10604933]

14. Weisstaub NV, et al. Cortical 5-HT2A receptor signaling modulates anxiety-like behaviors in mice. Science 2006;313:536–40. [PubMed: 16873667]

15. Benneyworth MA, et al. A selective positive allosteric modulator of metabotropic glutamate receptor subtype 2 blocks a hallucinogenic drug model of psychosis. Mol Pharmacol 2007;72:477–84. [PubMed: 17526600]

16. Angers S, Salahpour A, Bouvier M. Dimerization: an emerging concept for G protein-coupled receptor ontogeny and function. Annu Rev Pharmacol Toxicol 2002;42:409–35. [PubMed: 11807178]

17. Lopez-Gimenez JF, Canals M, Pediani JD, Milligan G. The alpha1b-adrenoceptor exists as a higher-order oligomer: effective oligomerization is required for receptor maturation, surface delivery, and function. Mol Pharmacol 2007;71:1015–29. [PubMed: 17220353]

18. Wright RA, Arnold MB, Wheeler WJ, Ornstein PL, Schoepp DD. [3H]LY341495 binding to group II metabotropic glutamate receptors in rat brain. J Pharmacol Exp Ther 2001;298:453–60. [PubMed: 11454905]

19. Palczewski K, et al. Crystal structure of rhodopsin: A G protein-coupled receptor. Science 2000;289:739–45. [PubMed: 10926528]

20. Fotiadis D, et al. Atomic-force microscopy: Rhodopsin dimers in native disc membranes. Nature 2003;421:127–8. [PubMed: 12520290]

21. Kenakin T. Efficacy at G-protein-coupled receptors. Nat Rev Drug Discov 2002;1:103–10. [PubMed: 12120091]

22. Gonzalez-Maeso J, Rodriguez-Puertas R, Meana JJ. Quantitative stoichiometry of G-proteins activated by mu-opioid receptors in postmortem human brain. Eur J Pharmacol 2002;452:21–33. [PubMed: 12323382]

23. Carlsson A. The neurochemical circuitry of schizophrenia. Pharmacopsychiatry 2006;39(Suppl 1):S10–4. [PubMed: 16508890]

24. Vollenweider FX, Geyer MA. A systems model of altered consciousness: integrating natural and drug-induced psychoses. Brain Res Bull 2001;56:495–507. [PubMed: 11750795]

25. Vollenweider FX, et al. Positron emission tomography and fluorodeoxyglucose studies of metabolic hyperfrontality and psychopathology in the psilocybin model of psychosis. Neuropsychopharmacology 1997;16:357–72. [PubMed: 9109107]

26. Umbricht D, et al. Effects of the 5-HT2A agonist psilocybin on mismatch negativity generation and AX-continuous performance task: implications for the neuropharmacology of cognitive deficits in schizophrenia. Neuropsychopharmacology 2003;28:170–81. [PubMed: 12496954]

27. Gouzoulis-Mayfrank E, et al. Inhibition of Return in the Human 5HT(2A) Agonist and NMDA Antagonist Model of Psychosis. Neuropsychopharmacology. 2005

28. Dean B. The cortical serotonin2A receptor and the pathology of schizophrenia: a likely accomplice. J Neurochem 2003;85:1–13. [PubMed: 12641722]

29. Davidson M, et al. Severity of symptoms in chronically institutionalized geriatric schizophrenic patients. Am J Psychiatry 1995;152:197–207. [PubMed: 7840352]

30. Gurevich EV, Joyce JN. Alterations in the cortical serotonergic system in schizophrenia: a postmortem study. Biol Psychiatry 1997;42:529–45. [PubMed: 9376449]

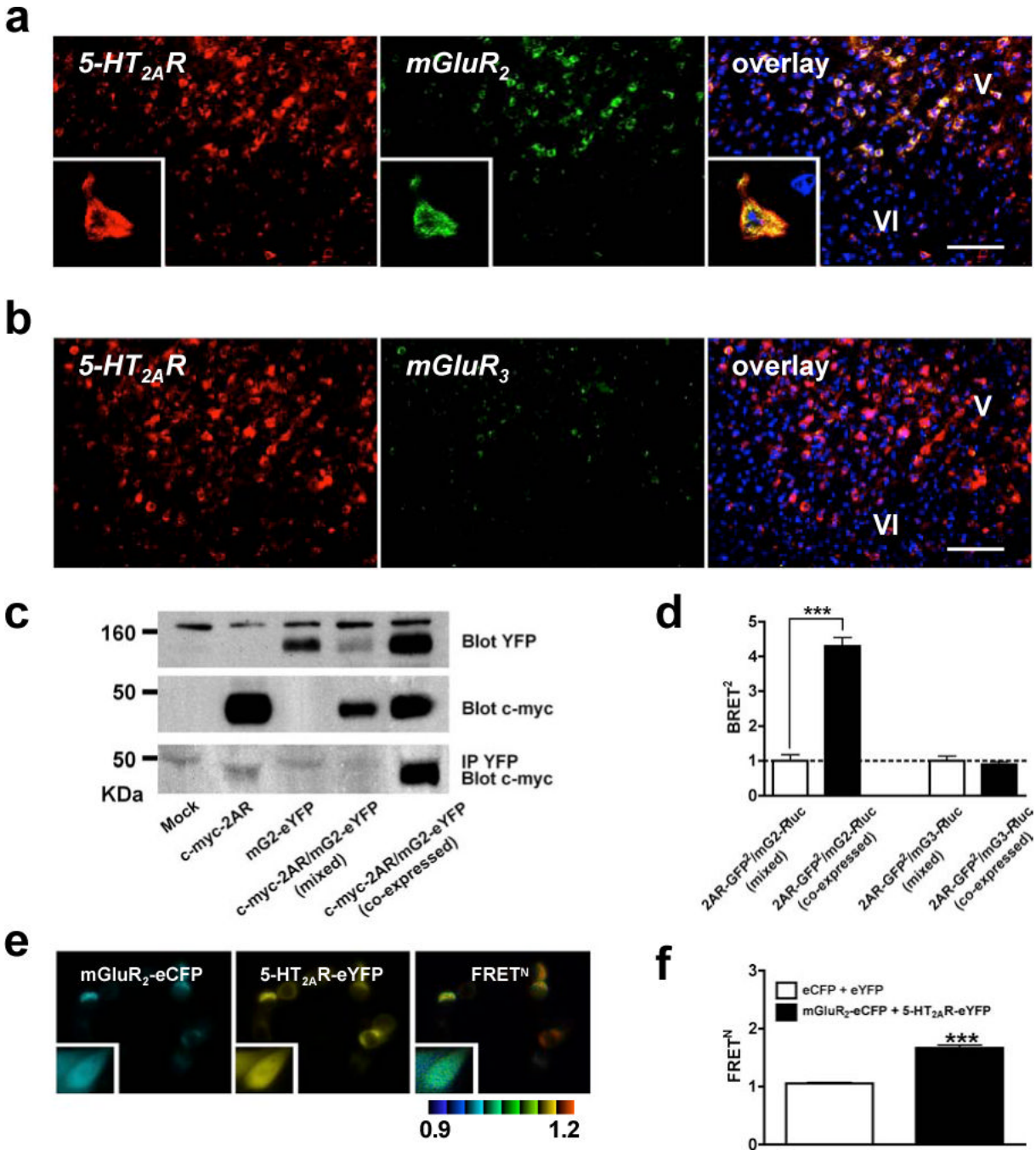

Figure 1. 2AR and mGluR2 co-localize and interact

a, *2AR* and *mGluR2*, but not *mGluR3*, co-express in neurons. Scale, top=50 μm, bottom=10 μm. Nuclei are blue. Inset: co-expressing neuron. **b,** FISH for *mGluR3* in thalamus. Scale, top=25μm, bottom=10μm. **c,** mRNA levels by real-time PCR (n=6 per group). **d,** Specific co-immunoprecipitation of 2AR and mGluR2 in duplicate human cortex samples (arrows). **e.** $BRET^2$ shows specific 2AR and mGluR2 interaction in HEK293 cells. Data are mean±s.e.m. (n=3). The mGluR2/2AR curve is preferably fitted by a saturation curve, F test ($p<0.001$). The other co-transfection datasets show linear correlations. **f**, [^{3}H]Ketanserin displacement curves in mouse SCx membranes (top panels). 2AR agonist affinities were higher in the presence of

mGluR2/3 agonist 10 μM LY379. [^{3}H]LY341495 displacement curves (bottom panels). mGluR2/3 agonist affinities were lower in the presence of 2AR agonist 10 μM DOI.

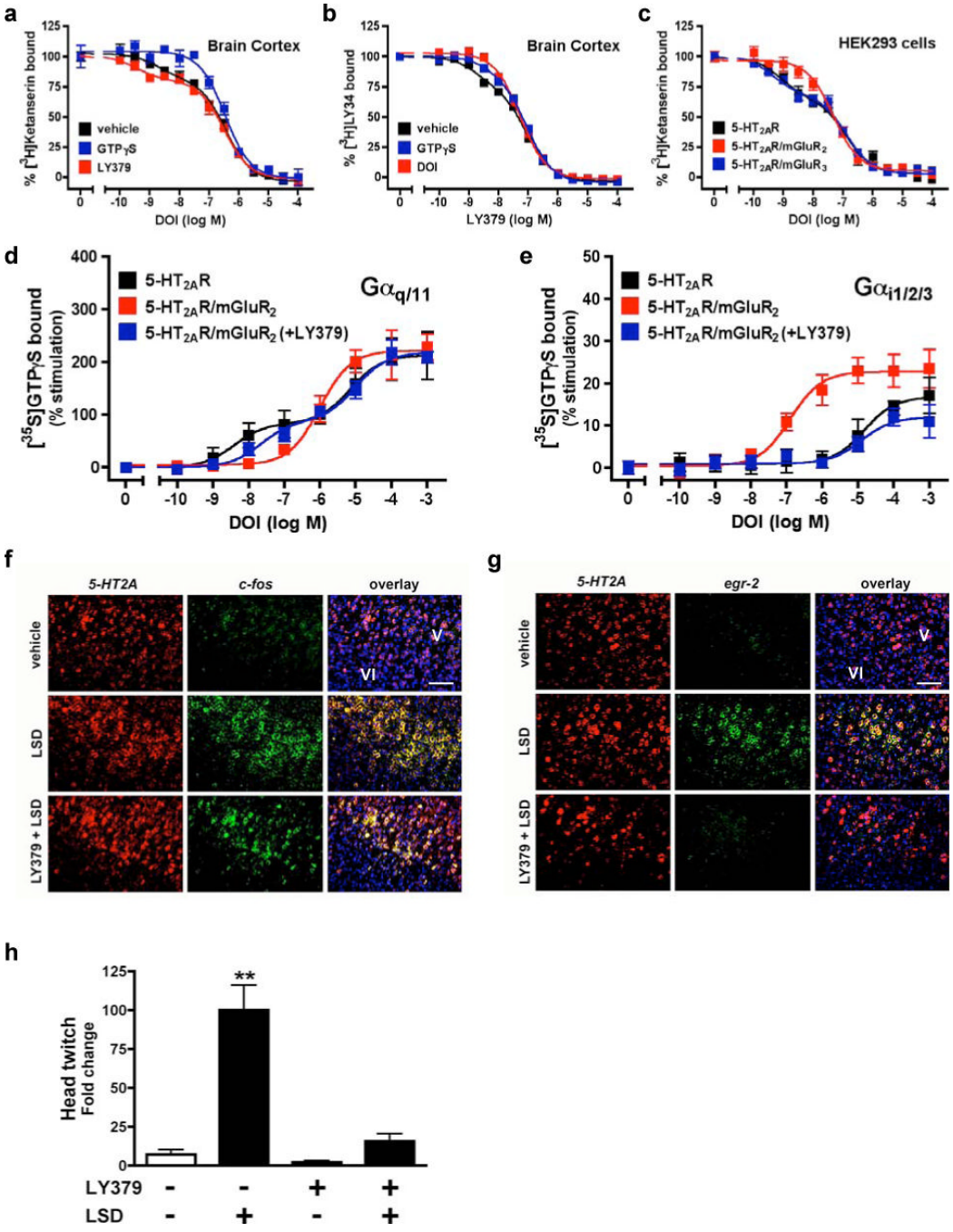

Figure 2. mGluR2 transmembrane domains 4/5 mediate association with 2AR

a, mGluR2/mGluR3 chimeras studied. **b,** c-myc-2AR and HA-mGluR2/mGluR3 chimera co-immunoprecipitations. Cells separately expressing each construct were also mixed. **c,** 2AR competition binding in cells stably expressing 2AR and transfected with mGluR2/mGluR3 chimeras. **d,** FRET in cells expressing 2AR-eCFP and either mGluR2, mGluR3 or mGluR3ΔTM4,5 chimera, all tagged with eYFP. Pseudo-colour images represent normalized values ($FRET^N$). eCFP + eYFP (n=19); 2AR-eCFP + mGluR2-eYFP (n=43); 2AR-eCFP + mGluR3-eYFP (n=31); 2AR-eCFP + mGluR3ΔTM4,5-eYFP, (n=27). **p < 0.01; ANOVA with Dunnett's *post hoc* test. **e,** DOI-stimulated [^{35}S]GTPγS binding in membranes followed by immunoprecipitation with anti-$G\alpha_{q/11}$ (top panels), or anti-$G\alpha_{i1,2,3}$ (bottom panels). Cells

stably expressing 2AR were transfected with mGluR2, mGluR3 or mGluR3ΔTM4,5. The potency of DOI activating $G\alpha_{i1,2,3}$ was significantly increased when the 2AR was co-expressed with either mGluR2 or mGluR3ΔTM4,5, an effect abolished by 10 μM LY379 ($p<0.001$ by F test). Data are mean±s.e.m. of three experiments performed in triplicate. **f,** Ribbon backbone representation of the transmembrane helices of the 2AR/mGluR2 heteromer model from the intracellular face.

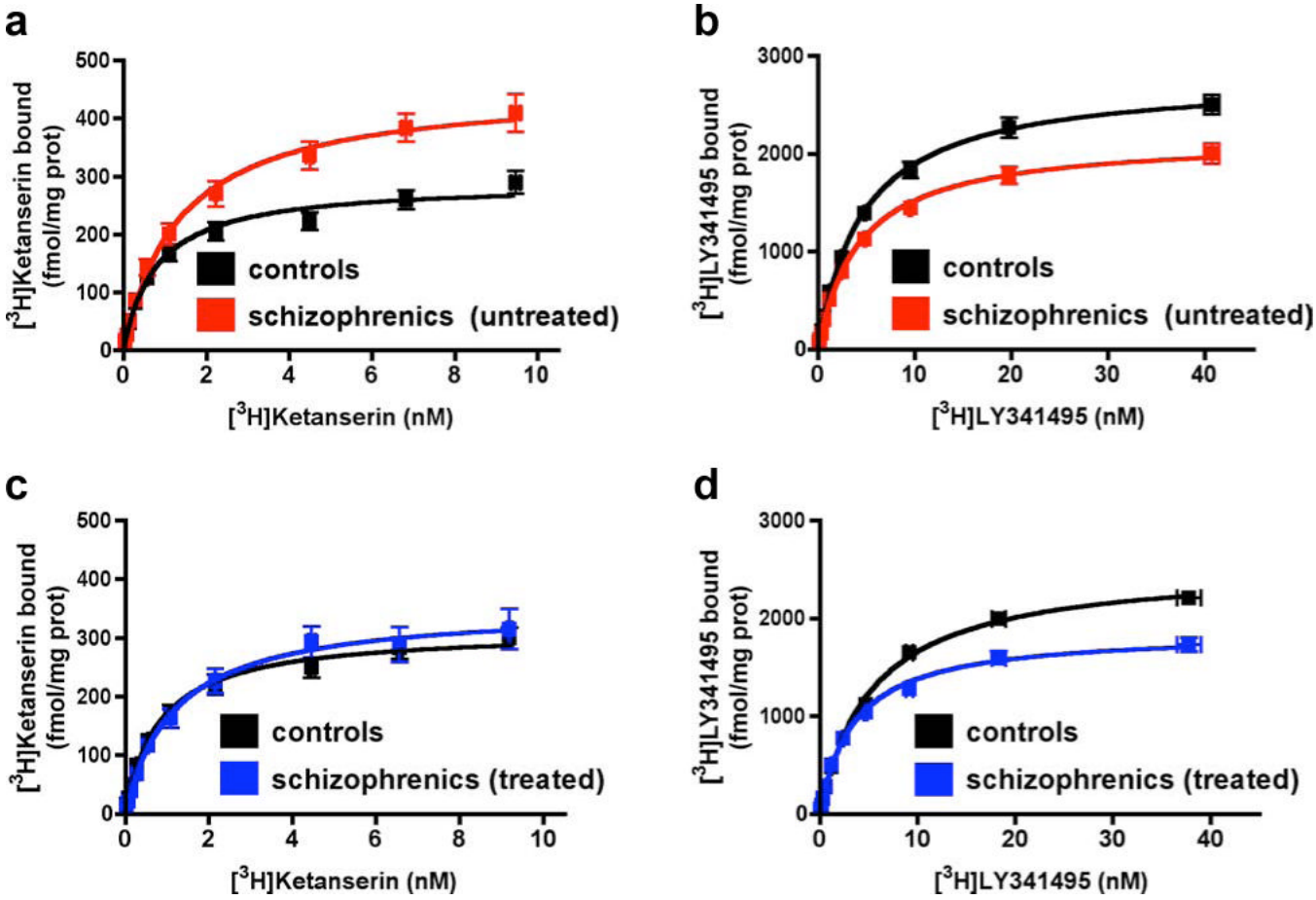

Figure 3. 2AR/mGluR2 complex-dependent modulation of cellular and behavioural responses

a , DOI-stimulated [^{35}S]GTPγS binding in primary culture membranes followed by immunoprecipitation with anti-G$\alpha_{q/11}$ or anti-G$\alpha_{i1,2,3}$ antibodies. DOI G$\alpha_{i1,2,3}$ activation potency was significantly decreased by 10 μM LY379. Data are mean±s.e.m. of three experiments performed in triplicate. **b,** FISH in mice injected with vehicle or 2 mg/kg DOI 15 min after being pre-injected with vehicle or 15 mg/kg LY379 (left panels), and in primary cultures treated with 10 μM DOI 15 min after being pre-treated with vehicle or 10 μM LY379 (bottom panels). Nuclei are blue. Scale, left=50 μm, right=10μm. **c,** Distance and vertical activity induced in *htr2A*+/+ and *htr2A*−/− mice by mGluR2/3 antagonist 6 mg/kg LY341495. In *htr2A*−/− mice, LY341495 effect on distance was reduced ($p<0.05$, Bonferroni's *post hoc* test of two-factor ANOVA), and on vertical activity was absent (n=30−32).

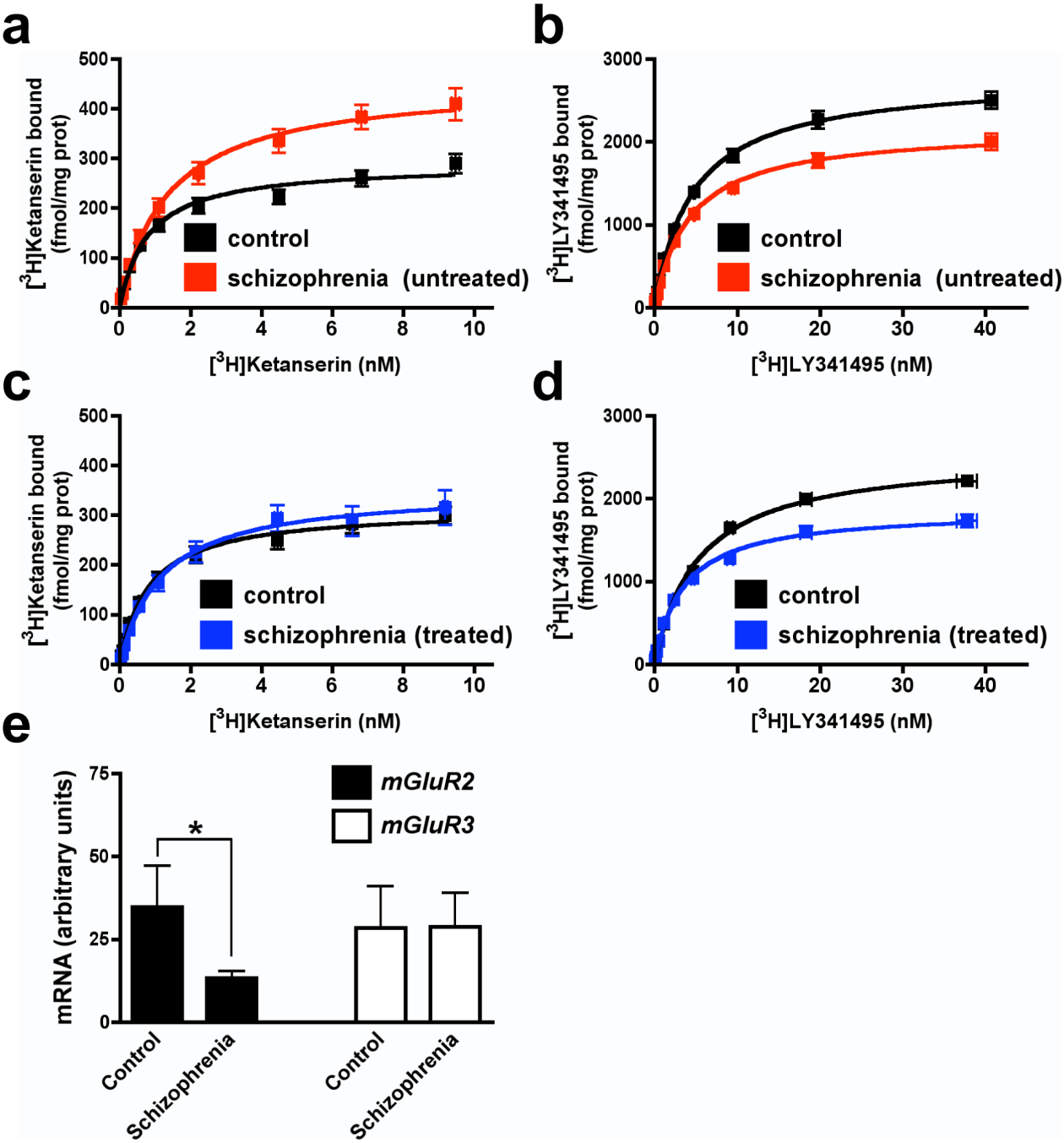

Figure 4. 2AR is increased and mGluR2 is decreased in schizophrenia

a, b, Frontal cortex membrane receptor binding assays from untreated schizophrenic (n = 13) and matched control subjects (n = 13). In schizophrenia, [^{3}H]ketanserin binding was higher and [^{3}H]LY341495 binding was lower ($p < 0.05$; Student's *t*-test). **c, d,** Receptor binding in antipsychotic-treated schizophrenic (n = 12) and matched control subjects (n = 12). In treated schizophrenia, [^{3}H]ketanserin binding was unaffected and [^{3}H]LY341495 binding was lower ($p < 0.05$). **e,** *mGluR2* mRNA expression is reduced in untreated schizophrenic subjects (n = 7) compared to matched control subjects (n = 7, $p < 0.05$, mean±s.e.m).

SUPPLEMENTARY METHODS

Materials and Drug Administration. 1-(2,5-dimethoxy-4-iodophenyl)-2-aminopropane (DOI), 1-(2,5-dimethoxy-4-methylphenyl)-2-aminopropane (DOM), 1-(2,5-dimethoxy-4-bromophenyl)-2-aminopropane DOB, lysergic acid diethylamide (LSD), and lisuride hydrogen maleate (lisuride) were purchased from Sigma-Aldrich. (1R,4R,5S,6R)-4-Amino-2-oxabicyclo[3.1.0]hexane-4,6-dicarboxylic acid (LY379268) was obtained from Eli Lilly and Company. 2S-2-amino-2-(1S,2S-2-carboxycyclopropan-1-yl)-3-(xanth-9-yl)-propionic acid (LY341495), (2S,2'R,3'R)-2-(2',3'-dicarboxycyclopropyl)-glycine (DCG-IV), (2S,1'S,2'S)-2-(carboxycyclopropyl)-glycine (L-CCG-I), clozapine, and haloperidol were obtained from Tocris Cookson Inc. [^{3}H]Ketanserin and [^{35}S]GTPγS were purchased from PerkinElmer Life and Analytical Sciences, Inc. [^{3}H]LY341495 was purchased from American Radiolabeled Chemicals, Inc. The injected doses (i.p.) were DOI, 2 mg/kg; DOM, 4 mg/kg; DOB, 1 mg/kg; LSD, 0.24 mg/kg; lisuride, 0.4 mg/kg; ergotamine, 0.5 mg/kg; LY379268, 15 mg/kg; LY341495, 6 mg/kg; clozapine, 25 mg/kg; and haloperidol, 1 mg/kg, unless otherwise indicated.

Transient Transfection of HEK293 cells. HEK293 were maintained in Dulbecco's modified Eagle's medium supplemented with 10% (v/v) foetal bovine serum at 37°C in a 5% CO_2 humidified atmosphere. Transfection was performed using Lipofectamine 2000 reagent (Invitrogen) according to manufacturer's instructions. HEK293 cells stably expressing human 2AR have been described previously[1,2].

Co-immunoprecipitation Studies. Co-immunoprecipitation studies in *postmortem* human brain, and co-immunoprecipitation studies using N-terminally c-myc tagged form of 2AR, and N-terminally haemagglutinin (HA) tagged forms of mGluR2, mGluR3 or mGluR2/mGluR3 chimeras in HEK293 were performed as previously described with minor modifications[3]. Briefly, the samples were incubated overnight with protein A/G beads and anti-2AR (*postmortem* human brain) or anti-c-myc antibody (HEK293 cells) at 4°C on a rotating wheel. Equal amounts of proteins were resolved by SDS-polyacrylamide gel electrophoresis. Detection of proteins by immunoblotting using anti-2AR (Santa Cruz Biotechnology), anti-mGluR2 and anti-mGluR3 (Abcam Inc.) in *postmortem* human brain, or anti-c-myc and anti-HA antibodies (Santa Cruz Biotechnology) in HEK293 was conducted using ECL system according to the manufacturer's recommendations.

Bioluminiscence Resonance Energy Transfer (BRET^2) in HEK293 live cells. The human 2AR, serotonin 5-HT$_{2C}$ (2CR), mGluR2, and mGluR3 receptors with mutated stop codons were subcloned into the p*R*luc and pGFP^2 plasmids (PerkinElmer Life Sciences), such that *Renilla* luciferase (*R*luc) and Green Fluorescent Protein (GFP^2) were present at the C-termini of the receptors. All sequences were confirmed by DNA sequencing. After 48 h, transfected cells were washed with PBS, suspended to 1-2 × 10^6 cells/ml, and were treated with DeepBlueC Coelenterazine Substrate (5 μM final concentration; PerkinElmer Life Sciences). Equivalents amounts of total DNA comprised of various ratios of the *R*luc- or GFP^2-tagged receptors were transfected[4]. Light emission was monitored

by using a Fusion Universal Microplate Analyzer (PerkinElmer Life Sciences). A $BRET^2$ signal is defined as the light emitted by GFP^2 at 515 nm in response to the light emitted at 410 nm by *R*luc in upon catalysis of DeepBlueC. The values were corrected by subtracting the background $BRET^2$ signal detected when the receptor-*R*luc construct was expressed alone (see Supplementary Fig. S3 for luminescence and fluorescence values). The specificity of mGluR2-*R*luc and 2AR-GFP^2 interactions were assessed by comparison with co-expression of mGluR2-*R*luc and 2CR-GFP^2, mGluR3-*R*luc and 2AR-GFP^2 and mGluR2-*R*luc and GFP^2. Data from a single experiment, which has been replicated three times, are displayed as mean±s.e.m. (Fig. 1e).

Fluorescence Resonance Energy Transfer (FRET). Forms of the 2AR and mGluR2 C-terminally fused to eCFP and eYFP were generated, and FRET microscopy in living cells was conducted as previously reported[3]. Results from a single experiment, representative of two-three independent studies, are shown in Fig. 2d.

[^{3}H]Ketanserin, [^{3}H]LY341495 and [^{35}S]GTPγS Binding. Membrane preparations and [^{3}H]ketanserin binding assays were performed as previously reported[5]. [^{3}H]LY341495 binding was performed as previously described with minor modifications[6]. Briefly, membrane preparations were incubated for 60 min at 4°C. Non-specific binding was determined in the presence of 1mM L-glutamate. [^{35}S]GTPγS binding experiments were initiated by the addition of membranes containing 35 μg protein to an assay buffer (20 mM HEPES, 3 mM $MgCl_2$, 100 mM NaCl, 0.2 mM ascorbic acid, and 0.5 nM [^{35}S]GTPγS)

supplemented with 0.1 μM or 10 μM GDP for $G\alpha_{q/11}$ and $G\alpha_i$, respectively, and containing the indicated concentration of ligands. Nonspecific binding was determined in the presence of 100 μM GTPγS. Reactions were incubated for 30 min at 30°C, and were terminated by the addition of 0.5 ml of ice-cold buffer, containing 20 mM HEPES, 3 mM $MgCl_2$, 100 mM NaCl, and 0.2 mM ascorbic acid. The samples were centrifuged at 16,000×g for 15 min at 4°C, and the resulting pellets resuspended in solubilization buffer (100 mM Tris, 200 mM NaCl, 1 mM EDTA, 1.25% Nonidet P-40) plus 0.2% sodium dodecylsulfate. Samples were precleared with Pansorbin (Calbiochem), followed by immunoprecipitation with antibody to $G\alpha_{q/11}$ or $G\alpha_{i1,2,3}$ (Santa Cruz Biotechnology). Finally, the immunocomplexes were washed twice with solubilization buffer, and bound [^{35}S]GTPγS was measured by liquid-scintillation spectrometry.

Construction of Receptor Chimeras.

All PCR reactions were performed using PfuTurbo Hotstart DNA polymerase (Stratagene, La Jolla, CA) in a PTC-100 thermal cycler (MJ Research, Waltham, MA). Cycling conditions were 30 cycles of 94 C/30 sec, 55 C/30 sec and 72 C/1 min per kilobase of amplicon, with an initial denaturation/activation of 94 C/2 min and a final extension of 72 C/7 min.

HA-tagged wild type human mGluR2 and mGluR3 constructs. The rat mGluR5 signal peptide (SP)[7] along with an HA epitope tag was PCR amplified using primers NheI-HA_SP/S (5'-TTTTgctagcGAATTCCTTTCCTAAAATGG-3') and HA_SP-KpnI/A (5'-TTTTggtaccACGCGTGGCGTAGTCGGGTA-3') with pRK5 as

template. Wild type human mGluR2 and mGluR3 were amplified using primers MluI-hGRM2/S (5'-agctacgcgtAAGAAGGTGCTGACCCTGGA-3') hGRM2-XbaI/A (5'-AAtctagaTCAAAGCGATGACGTTGTCGAG-3') and KpnI-hGRM3/S (5'-acgtggtaccTTAGGGGACCATAACTTTCT-3') hGRM3-XhoI/A (5'-acgtctcgagTCACAGAGATGAGGTGGTGG-3'), respectively. The rat mGluR5 signal peptide/HA epitope fragment was digested with NheI and MluI, the human mGluR2 fragment was digested with MluI and XbaI, and were simultaneously subcloned into the NheI and XbaI sites of pcDNA3.1 (Invitrogen, Carlsbad, CA) to yield the HA-tagged mGluR2 construct. Similarly, the rat mGluR5 signal peptide/HA fragment was digested with NheI and KpnI, the human mGluR2 PCR product was digested with KpnI and XhoI, and were simultaneously subcloned into the NheI and XhoI sites of pcDNA3.1 to give the HA-tagged mGluR2 construct.

Chimeric human mGluR2 with transmembrane domain 4 and 5 from human mGluR3. Fragment of the transmembrane domain TM1 to the C terminus of the second intracellular loop of the human mGluR2 was amplified using primers hGRM2-1476/S (5'-GGACACCAGCCTCATCCCAT-3') and hGRM2i2GRM3TM4/A (5'-CAGATGAAAACCTGAGAACTAGGACTGATGAAGCGTGGCC-3'). Fragment of the TM4 through TM5 of the human mGluR3 was amplified using primers hGRM2i2GRM3TM4/S (5'-GGCCACGCTTCATCAGTCCTAGTTCTCAGGTTTTCATCTG-3') and hGRM3TM5GRM2i3/A (5'-

TTTTCGGGGCACTTGCGAGTTTTGAAGGCGTACACAGTGC-3'). The two fragments were annealed and re-amplified using primers hGRM2-1476/S and hGRM3TM5GRM2i3/A. The third intracellular loop to the carboxyl terminal of the human mGluR2 was amplified using primers hGRM3TM5GRM2i3/S (5'-GCACTGTGTACGCCTTCAAAACTCGCAAGTGCCCCGAAAA-3') and hGRM2-XbaI/A. This fragment was then annealed with the previous PCR product and re-amplified using primers hGRM2-1476/S and hGRM2-XbaI/A. To reconstitute the complete chimeric receptor, the N terminal domain of the HA-tagged wild type human mGluR2 was released using NheI and BstBI, the final PCR product was digested using BstBI and XbaI, and the two fragments were simultaneously subcloned into the NheI and XbaI sites of pcDNA3.1.

Chimeric human mGluR3 with transmembrane domain 4 and 5 from human mGluR2. Fragment of the transmembrane domain TM1 to the C terminus of the second intracellular loop of the human mGluR3 was amplified using primers hGRM3-2541/S (5'- TGAAAGTTGGTCACTGGGCA-3') and hGRM3i2GRM2TM4/A (5'-CAGATGGCCACCTGTGAGGCGGGGCTGATGAATTTTGGCC-3'). Fragment of the TM4 through TM5 of the human mGluR2 was amplified using primers hGRM3i2GRM2TM4/S (5'-GGCCAAAATTCATCAGCCCCGCCTCACAGGTGGCCATCTG-3') and hGRM2TM5GRM3i3/A (5'-TTTTCTGGGCACTTCCGCGTCTTGAAGGCATAAAGCGTGC-3'). The two fragments were annealed and re-amplified using primers hGRM3-2541/S and

hGRM2TM5GRM3i3/A. The third intracellular loop to the carboxyl terminal of the human mGluR3 was amplified using primers hGRM2TM5GRM3i3/S (5'-GCACGCTTTATGCCTTCAAGACGCGGAAGTGCCCAGAAAA-3') and hGRM3-XhoI/A. This fragment was then annealed with the previous PCR product and re-amplified using primers hGRM3-2541/S and hGRM3-XhoI/A. To reconstitute the complete chimeric receptor, the N terminal domain of the HA-tagged wild type human mGluR3 was released using NheI and PstI, the final PCR product was digested using PstI and XhoI, and the two fragments were simultaneously subcloned into the NheI and XhoI sites of pcDNA3.1.

Chimeric human mGluR3 with transmembrane domain 1 through 5 from human mGluR2. A small fragment of the N terminal domain to the beginning of TM1 of the human mGluR3 was amplified using primers hGRM3-2541/S and hGRM3NGRM2TM1/A (5'-ACAGCCCAGGCATCGCCCCAGCGGATGTAGTCCTCAGGAAGGT-3'). Fragment of the TM1 through TM5 of the human mGluR2 was amplified using primers hGRM3NGRM2TM1/S (5'-ACCTTCCTGAGGACTACATCCGCTGGGGCGATGCCTGGGCTGT-3') and hGRM2TM5GRM3i3/A. The two fragments were annealed and re-amplified using primers hGRM3-2541/S and hGRM2TM5GRM3i3/A. The third intracellular loop to the carboxyl terminal of the human mGluR3 was amplified using primers hGRM2TM5GRM3i3/S and hGRM3-XhoI/A. This fragment was then annealed with the previous PCR product and re-amplified using primers hGRM3-2541/S and hGRM3-XhoI/A. To reconstitute the complete chimeric receptor, the N

terminal domain of the HA-tagged wild type human mGluR3 was released using NheI and PstI, the final PCR product was digested using PstI and XhoI, and the two fragments were simultaneously subcloned into the NheI and XhoI sites of pcDNA3.1.

Molecular modelling. Three-dimensional molecular models of the seven transmembrane (TM) regions of 2AR and mGluR2 were built using the crystal structures of β_2-adrenergic receptor[8] and rhodopsin[9], respectively, as structural templates, and the latest version of the homology-modeling program MODELLER[10]. The use of the very recent crystal structure of β_2-adrenergic receptor to build a model of 2AR is justified by the higher sequence identity between these two receptors compared to rhodopsin, and the suitability of the rhodopsin template to build models of family C GPCRs, which includes the mGluR2, has recently been discussed in the literature[11]. The sequence alignment between the transmembrane helices of β_2-adrenergic receptor and 2AR was obtained with BLAST[12]. For mGluR2, we used the same alignment with rhodopsin as described in Binet et al. (2007)[11]. A multiple alignment of available mGluR2 and mGluR3 sequences was performed with the CLUSTALW program version 1.81[13]. Supplementary Fig. S7 shows the details of these sequence alignments in the transmembrane regions.

To build a reasonable configuration of the 2AR-mGluR2, we used the TM4,5-TM4,5 configuration deriving from atomic force microscopy of rhodopsin in native disk membranes[14] as a template for the heteromer interface between 2AR and mGluR2. This modeling was obtained with the assistance of the Insight II User

Graphical Interface (Accelrys Inc.) on a graphics workstation.

Neuronal primary culture. Primary cultures of cortical and thalamic neurons were prepared as previously described[5].

Mouse brain samples. Experiments were performed as previously described[5] on adult (8–12 weeks old) male 129S6/Sv mice. For experiments involving genetically modified mice, *htr2A+/+* or *htr2A+/-* littermates were used as controls[5,16]. Animals were housed at 12 h light/dark cycle at 23°C with food and water *ad libitum*. The Institutional Animal Use and Care Committee approved all experimental procedures at Mount Sinai School of Medicine and Columbia University.

Fluorescence *in situ* hybridization (FISH). Synthesis of modified DNA oligonucleotide probes, probe labeling, and fluorescence *in situ* hybridization was performed as previously described[5,15]. See Supplementary Table S10 for oligonucleotide probe sequences.

Quantitative real-time PCR. Quantitative real-time PCR (qRT-PCR) experiments were performed as previously described[5]. See Supplementary Tables S11 and S12 for primer pair sequences.

Behavioural Studies. Behavioural studies were performed as previously described[5,16]. Motor function was assessed using a computerized three-dimentional activity monitorin system (AccuScan Instruments). The activity monitor has 32 infrared sensor pairs with 16 along each side spaced 2.5 cm apart. The system determines motor activity based on the frequency of interruptions to infrared beams traversing the *x*, *y* and *z* planes. Total distance

(cm) travelled and vertical activity were automatically determined from the interruptions of beams in the horizontal and vertical planes, respectively.

Brain Samples. Human brains were obtained at autopsies performed in the Forensic Anatomical Institute, Bilbao, Spain. The study was developed in compliance with policies of research and ethical review boards for postmortem brain studies (Basque Institute of Legal Medicine, Spain). Deaths were subjected to retrospective searching for previous medical diagnosis and treatment using examiner's information and records of hospitals and mental health centers. After searching of *antemortem* information was fulfilled, 25 subjects who had met criteria of schizophrenia according to the Diagnostic and Statistical Manual of Mental Disorders (DSM-IV)[17] were selected. A toxicological screening for antipsychotics, other drugs and ethanol was performed on blood, urine, liver and gastric contents samples. All subjects who were drug-free before death (as revealed by the absence of prescriptions in medical histories) also gave negative results in the toxicological screening. The toxicological assays were performed at the National Institute of Toxicology, Madrid, Spain, using a variety of standard procedures including radioimmunoassay, enzymatic immunoassay, high-performance liquid chromatography and gas chromatography-mass spectrometry. Controls for the present study were chosen among the collected brains on the basis, whenever possible, of the following cumulative criteria: (1) negative medical information on the presence of neuropsychiatric disorders or drug abuse; (2) appropriate gender, age and *postmortem* delay to match each subject in the schizophrenia group; (3) sudden and unexpected death (motor

vehicle accidents); and (4) toxicological screening for psychotropic drugs with negative results except for ethanol. Tissue pH is assumed to be an indicator of agonal status[18].Thus, prolonged terminal hypoxia results in low tissular pH. It has been demonstrated that gene expression patterns are strongly dependent on tissue pH. Brief deaths, associated with accidents, cardiac events or asphyxia, generally had normal pH with minor influence on gene expression changes[19]. All schizophrenic and control subjects showed a sudden and rapid death without long agonal phase. The tissue storage period before assays did not differ between schizophrenic cases (82 ± 9 months) and controls (85 ± 10 months). Specimens of prefrontal cortex (Brodmann's area 9) were dissected at autopsy (0.5-1 g tissue) on an ice-cooled surface and immediately stored at -70°C until membrane preparation. The definitive pairs of antipsychotic-untreated schizophrenics and respective matched controls are shown in Supplementary Table S8, and the definitive pairs of antipsychotic-treated schizophrenics and respective matched controls are shown in Supplementary Table S9.

SUPPLEMENTARY FIGURE LEGENDS

Figure S1. Evaluation of the specificity of FISH assay. **a,** FISH assay for *2AR* and *β-actin* in *htr2A+/+* and *htr2A-/-* mouse SCx. Red, green, and blue colours indicate *2AR*, *β-actin*, and nucleus (DAPI), respectively. **b,** Competition of *2AR*, *mGluR2* and *mGluR3* hybridization by specific, unlabeled oligonucleotide probes. A FISH assay in mouse SCx (*2AR* and *mGluR2*) and in mouse thalamus (*mGluR3*) with the fluorescently labelled oligonucleotides used in Fig. 1 was performed with the inclusion of excess of unlabeled oligonucleotides in the hybridization buffers. The presence of specific unlabeled oligonucleotides completely eliminated the signal obtained with the fluorescently labeled oligonucleotide probes. Red, green, and blue colours indicate *2AR*, *mGluR2* or *mGluR3*, and nucleus (DAPI), respectively. **c,** Similar anatomical pattern of expression of mGluR2 in mouse SCx was obtained with two different sets of fluorescently labeled oligonucleotide probes, and with the combination of probe set 1 and probe set 2. Green, and blue colours indicate *mGluR2* and nucleus (DAPI), respectively. **d,** Evaluation of FISH assay specificity using scrambled-sequence oligonucleotide probes. FISH was performed by using a mixture of five fluorescently-labeled scrambled oligonucleotide probes. Scale bar, 500 μm. See Supplementary Table S10 for oligonucleotide sequences.

Figure S2. Lower expression of mGluR2 in the absence of cortical 2AR. **a,** Schematic representation of *htr2A+/+*, *htr2A-/-*, *htr2A-/-:Emx-Cre*, and *htr2A-/-:Htt-Cre* mice. Note that in *htr2A-/-:Emx-Cre* mice (cortical rescue), 2AR is only expressed in cortical pyramidal neurons, and in *htr2A-/-:Htt-Cre* mice (thalamic

rescue), 2AR is only expressed in thalamic neurons. **b, c,** [^{3}H]LY341495 binding saturation curves in mouse SCx membranes (n = 6 per group). B_{max} values were significantly lower in *htr2A-/-* mice ($p < 0.001$; Student's *t*-test), and in *htr2A-/-:Htt-Cre* mice ($p < 0.001$; ANOVA with Bonferroni's post hoc test). **d,** Expression of *mGluR2* and *mGluR3* mRNA in mouse SCx in *htr2A+/+* (black), *htr2A-/-* (white), *htr2A+/-* (blue), *htr2A-/-:Emx-Cre* (red), and *htr2A-/-:Htt-Cre* (green) mice assayed by qRT-PCR (n = 6-12 per group). Expression level was significantly lower for *mGluR2* in *htr2A-/-* mice ($p < 0.001$; Student's *t*-test), and in *htr2A-/-:Htt-Cre* mice ($p < 0.05$; ANOVA with Bonferroni's post hoc test).

Figure S3. Intact HEK293 cells transiently transfected with (**a**) increasing amounts of mGluR2-*R*luc or mGluR3-*R*luc or (**b**) with increasing amounts of 2AR-GFP^2, 2CR-GFP^2 or pGFP^2. The amount of each cDNA is noted. Donor (**a**) and acceptor (**b**) conjugate relative expression levels were monitored by measuring luminescence and fluorescence. Note that the signals detected are comparable for different donors and acceptors. Data from triplicates assays in a single experiment are displayed. Two further experiments produced similar results.

Figure S4. [^{3}H]Ketanserin binding displacement curves by DOI, DOM and DOB in mouse SCx membranes (top panels). Note that the affinity of DOI displacing [^{3}H]ketanserin binding was significantly higher in the presence of 10μM LY379, (see Supplementary Table S2). [^{3}H]LY341495 binding displacement curves by LY379, DCG-IV and L-CCG-I in mouse SCx membranes (bottom panels). Note that the affinity of LY379, DCG-IV and L-CCG-I displacing [^{3}H]LY341495 binding

was significantly lower in the presence of 10μM DOI (see Supplementary Table S3).

Figure S5. [^{3}H]Ketanserin binding and [^{3}H]LY341495 binding in HEK293 cells stably expressing 2AR and transfected with mock, mGluR2 or mGluR3. **a,** [^{3}H]Ketanserin binding saturation curve in HEK293 cells stably expressing 2AR. **b,** [^{3}H]LY341495 binding saturation curves in HEK293 cells stably expressing 2AR and transfected with mock (open squares), 1 μg (filled triangles), 3 μg (inverted filled triangles), 6 μg (filed diamonds) , 12 μg (filled circles), or 24 μg mGluR2-eYFP (filled squares), or 24 μg mGluR3-eYFP (opened triangles). See Supplementary Table S4 for receptor densities. Note that [^{3}H]Ketanserin and [^{3}H]LY341495 B_{max} values in mouse SCx were 572±50 fmol/mg prot. and 2986±64 fmol/mg prot., respectively, and that [^{3}H]Ketanserin and [^{3}H]LY341495 B_{max} values in cortical primary cultures were 404±12 fmol/mg prot. and 1246±34 fmol/mg prot., respectively. **c,** [^{3}H]Ketanserin binding displacement curves in HEK293 cells stably expressing 2AR and transfected with mock, 24 μg of mGluR2-eYFP (left panels), or 24 μg mGluR3-eYFP (right panels). See Supplementary Table S4 for pharmacological parameters.

Figure S6. Characterization of mGluR2/mGluR3 chimeras. **a,** N-terminally HA-tagged mGluR2, mGluR3 and mGluR2/mGluR3 chimeras were expressed in HEK293 cells, fixed and stained with anti-HA antibody. **b**, [^{3}H]LY341495 binding saturation curves in HEK293 cells transfected with mock, mGluR2, mGluR3 and mGluR2/mGluR3 chimeras. Note that the level of expression is comparable for the different constructs (see also Supplementary Fig. S5). **c,** [^{3}H]Ketanserin

binding displacement curves by DOI in HEK293 cells stably expressing 2AR and transfected with mock mGluR2, mGluR3 and mGluR2/mGluR3 chimeras. Note that the 2AR affinity for DOI was decreased by mGluR2, ΔmGluR2, mGluR3ΔTM1-5 and mGluR3ΔTM4,5 co-expression, and was unaffected by mGluR3 and mGluR2ΔTM4,5 co-expression (see also Fig. 2 and Supplementary Table S5).

Figure S7. Multiple sequence alignment of the transmembrane regions of mGluR2 and mGluR3 with those of 2AR, β_2-adrenergic receptor and rhodopsin. All residues are identified by the generic numbering system for rhodopsin-like GPCR sequences as well as by the residue numbers of the amino acidic sequences of the cloned human and rat mGluR2 (MGR2_HUMAN and MGR2_RAT, respectively), human, *Pongo pygmaeus*, mouse and rat mGluR3 (MGR3_HUMAN, MGR3_PONPY, MGR3_MOUSE, and MGR3_RAT, respectively), human 2AR (5HT2A_HUMAN), human β_2-adrenergic receptor (B2AR_HUMAN), and bovine rhodopsin (OPSD_BOVIN).

Fig S8. Double-label FISH was performed in SCx layers V and VI in mice injected (i.p.) with vehicle or 0.24 mg/kg LSD 15 min after being pre-injected with vehicle or 15 mg/kg LY379. Red, green, and blue colours indicate *2AR*, *c-fos* (**a**) or *egr-2* (**b**), and nucleus (DAPI), respectively. Note that the induction of the hallucinogen signalling marker *egr-2* is selectively attenuated by LY379 in mouse SCx. Scale bar, 60 μm.

Figure S9. Activation of mGluR2 inhibits the specific cellular responses induced by 2AR agonists in mouse SCx. Dose-response curves of LY379 on cellular

response induced by 2AR agonists in mouse SCx assayed by qRT-PCR. Mice were injected with vehicle, 2 mg/kg DOI, 4 mg/kg DOM, 1 mg/kg DOB, 0.24 mg/kg LSD, 0.4 mg/kg lisuride, or 0.5 mg/kg ergotamine 15 min after being pre-injected with vehicle or 15 mg/kg LY379 (n = 4-12 per group). Note that the induction of the hallucinogenic genomic marker *egr-2* is selectively attenuated by LY379. Data are means±s.e.m. Bonferroni's post hoc test of two-factor ANOVA. *p < 0.05, **p < 0.01, ***p < 0.001.

Figure S10. Activation of mGluR2 inhibits the specific cellular responses induced by 2AR agonists in cortical primary cultures. Cortical primary cultures were treated for 45 min with vehicle, 10 μM DOI, 10 μM LSD or 10 μM lisuride after being pre-treated for 15 min with vehicle or LY379 (n = 4-12 per group). Note that the induction of the hallucinogenic genomic marker *egr-2* is selectively attenuated by LY379. Data are means±s.e.m. Bonferroni's post hoc test of two-factor ANOVA. *p < 0.05, **p < 0.01, ***p < 0.001.

Figure S11. Head twitch response was determined in mice injected with vehicle, 2 mg/kg DOI or 0.24 mg/kg LSD 15 min after being pre-injected with 15 mg/kg LY379 (n = 5-12 per group). Data are means±s.e.m. ANOVA with Bonferroni's post hoc test. *p < 0.05, **p < 0.01, ***p < 0.001.

Figure S12. Chronic clozapine modulates the expression of the components of the 2AR/mGluR2 complex in mouse SCx. Animals were chronically (21 days) injected with vehicle (black) or 25 mg/kg clozapine (red) and sacrificed 1 day after the last clozapine injection. **a,** [^{3}H]Ketanserin binding in mouse SCx after vehicle or chronic clozapine (n = 6 per group). **b, c,** [^{3}H]LY341495 binding in

htr2A+/+ (b) or *htr2A-/-* (c) mouse SCx after vehicle or chronic clozapine (n = 6 per group). **d,** Expression of *2AR*, *mGluR2*, and *mGluR3* mRNA in mouse SCx assayed by qRT-PCR in *htr2A+/+* and *htr2A-/-* mice after vehicle or chronic clozapine (n = 6-12 per group). Data are means±s.e.m. *p < 0.05, **p < 0.01, ***p < 0.001; Student's *t*-test.

Figure S13. Chronic haloperidol does not affect the expression of the components of the 2AR/mGluR2 in mouse SCx. Animals were chronically (21 days) injected with vehicle (black) or 1 mg/kg haloperidol (red) and sacrificed 1 day after the last haloperidol injection. **a,** [^{3}H]Ketanserin binding in mouse SCx after vehicle or chronic haloperidol (n = 6 per group). **b,** [^{3}H]LY341495 binding in mouse SCx after vehicle or chronic haloperidol (n = 6 per group).

Figure S14. Age-related changes in [^{3}H]ketanserin (a, b) and [^{3}H]LY341495 (c, d) binding to cortical membranes of control subjects . **a, c,** Representative saturation curves. Data correspond to a 21-year-old subject (black) and an 86-year-old subject (white). **b, d,** [^{3}H]ketanserin (b) and [^{3}H]LY379268 (d) binding B_{max} values expressed in linear relation to the age of control subjects. Estimated linear regressions are represented. Statistical values represent Pearson's correlation coefficients between binding B_{max} values and age (n = 35).

SUPPLEMENTARY REFERENCES

1. Ebersole, B. J., Visiers, I., Weinstein, H. & Sealfon, S. C. Molecular basis of partial agonism: orientation of indoleamine ligands in the binding pocket of the human serotonin 5-HT2A receptor determines relative efficacy. *Mol Pharmacol* **63,** 36-43 (2003).
2. Gonzalez-Maeso, J. *et al.* Transcriptome fingerprints distinguish hallucinogenic and nonhallucinogenic 5-hydroxytryptamine 2A receptor agonist effects in mouse somatosensory cortex. *J Neurosci* **23,** 8836-43 (2003).
3. Lopez-Gimenez, J. F., Canals, M., Pediani, J. D. & Milligan, G. The alpha1b-adrenoceptor exists as a higher-order oligomer: effective oligomerization is required for receptor maturation, surface delivery, and function. *Mol Pharmacol* **71,** 1015-29 (2007).
4. James, J. R., Oliveira, M. I., Carmo, A. M., Iaboni, A. & Davis, S. J. A rigorous experimental framework for detecting protein oligomerization using bioluminescence resonance energy transfer. *Nat Methods* **3,** 1001-6 (2006).
5. Gonzalez-Maeso, J. *et al.* Hallucinogens Recruit Specific Cortical 5-HT(2A) Receptor-Mediated Signaling Pathways to Affect Behavior. *Neuron* **53,** 439-52 (2007).
6. Wright, R. A., Arnold, M. B., Wheeler, W. J., Ornstein, P. L. & Schoepp, D. D. [3H]LY341495 binding to group II metabotropic glutamate receptors in rat brain. *J Pharmacol Exp Ther* **298,** 453-60 (2001).

7. Blahos, J., 2nd *et al.* Extreme C terminus of G protein alpha-subunits contains a site that discriminates between Gi-coupled metabotropic glutamate receptors. *J Biol Chem* **273,** 25765-9 (1998).

8. Cherezov, V. *et al.* High-resolution crystal structure of an engineered human beta2-adrenergic G protein-coupled receptor. *Science* **318,** 1258-65 (2007).

9. Li, J., Edwards, P. C., Burghammer, M., Villa, C. & Schertler, G. F. Structure of bovine rhodopsin in a trigonal crystal form. *J Mol Biol* **343,** 1409-38 (2004).

10. Sali, A. & Blundell, T. L. Comparative protein modelling by satisfaction of spatial restraints. *J Mol Biol* **234,** 779-815 (1993).

11. Binet, V. *et al.* Common structural requirements for heptahelical domain function in class A and class C G protein-coupled receptors. *J Biol Chem* **282,** 12154-63 (2007).

12. Altschul, S. F., Gish, W., Miller, W., Myers, E. W. & Lipman, D. J. Basic local alignment search tool. *J Mol Biol* **215,** 403-10 (1990).

13. Thompson, J. D., Higgins, D. G. & Gibson, T. J. CLUSTAL W: improving the sensitivity of progressive multiple sequence alignment through sequence weighting, position-specific gap penalties and weight matrix choice. *Nucleic Acids Res* **22,** 4673-80 (1994).

14. Liang, Y. *et al.* Organization of the G protein-coupled receptors rhodopsin and opsin in native membranes. *J Biol Chem* **278,** 21655-62 (2003).

15. Chan, P., Yuen, T., Ruf, F., Gonzalez-Maeso, J. & Sealfon, S. C. Method for multiplex cellular detection of mRNAs using quantum dot fluorescent in situ hybridization. *Nucleic Acids Res* **33,** e161 (2005).

16. Weisstaub, N. V. *et al.* Cortical 5-HT2A receptor signaling modulates anxiety-like behaviors in mice. *Science* **313,** 536-40 (2006).

17. American Psychiatric Association. Diagnostic and Statistical Manual of Mental Disorders: DSM-IV 4th edition (Washington , DC, 1994).

18. Preece, P. & Cairns, N. J. Quantifying mRNA in postmortem human brain: influence of gender, age at death, postmortem interval, brain pH, agonal state and inter-lobe mRNA variance. *Brain Res Mol Brain Res* **118,** 60-71 (2003).

19. Li, J. Z. *et al.* Systematic changes in gene expression in postmortem human brains associated with tissue pH and terminal medical conditions. *Hum Mol Genet* **13,** 609-16 (2004).

Supplementary Table S1. Relative mRNA expression levels (*htr2A-/-* over *htr2A+/+*) of metabotropic glutamate receptors in mouse SCx estimated by qRT-PCR. See Supplementary Table 12 for GenBank accession numbers and primer sequences.

Gene Name	Fold change
grm1	0.98 ± 0.07
grm2	0.75 ± 0.03*
grm3	1.03 ± 0.09
grm4	1.17 ± 0.11
grm5	0.94 ± 0.06
grm6	N.D.
grm7	0.97 ± 0.08
grm8	0.91 ± 0.07

*p<0.001, Student's *t*-test, n = 12-44. N.D., not detected

Supplementary Table S2.

[^{3}H]Ketanserin binding displacement curves by DOI in mouse SCx membranes.

Ligand	$K_{i\text{-}high}$ (log M)	$K_{i\text{-}low}$ (log M)	% High
vehicle	-8.9 ± 0.2	-6.8 ± 0.07	20 ± 3
LY379 0.1μM	-8.9 ± 0.3	-6.7 ± 0.08	19 ± 4
LY379 1μM	-9.4 ± 0.3	-6.7 ± 0.09	26 ± 4
LY379 10μM	-9.7 ± 0.2*	-6.7 ± 0.06	23 ± 3
LY379 10μM + LY34	-8.8 ± 0.2	-6.6 ± 0.07	20 ± 3
GTPγS	NA	-6.8 ± 0.05	NA

DOI displacement of [^{3}H]ketanserin (2 nM; K_D = 2.72 nM) binding was performed in the absence (vehicle) or in the presence of LY379, LY34 (1 μM) or GTPγS (10 μM). Competition curves were analysed by nonlinear regression to derive dissociation constants for the high- ($K_{i\text{-}high}$), and the low- ($K_{i\text{-}low}$) affinity states of the receptor. % High refers to the percentage of high-affinity binding sites as calculated from nonlinear fitting. Values are best fit ± S.E. of 3-6 experiments performed in duplicate. One-site model or two-site model as a better description of the data was determined by *F* test. Two-site model, $p < 0.001$. NA, two-site model not applicable ($p > 0.05$). DOI displacement curve of [^{3}H]ketanserin with 10 μM LY379 compared to DOI displacement curve of [^{3}H]ketanserin with vehicle: $F[5,268] = 4.97$, *$p < 0.001$.

[^{3}H]Ketanserin binding displacement curves by DOM in mouse SCx membranes.

Ligand	$K_{i\text{-}high}$ (log M)	$K_{i\text{-}low}$ (log M)	% High
vehicle	-8.1 ± 0.3	-6.2 ± 0.09	18 ± 5
LY379 0.1μM	-8.4 ± 0.3	-6.1 ± 0.11	23 ± 8
LY379 1μM	-8.5 ± 0.1	-6.0 ± 0.07	29 ± 2*
LY379 10μM	-8.7 ± 0.2	-6.0 ± 0.06	32 ± 2**
LY379 10μM + LY34	-8.4 ± 0.4	-6.2 ± 0.11	17 ± 4
GTPγS	NA	-6.4 ± 0.07	NA

DOM displacement of [^{3}H]ketanserin (2 nM; K_D = 2.72 nM) binding was performed in the absence (vehicle) or in the presence of LY379, LY34 (1 μM) or GTPγS (10 μM). Competition curves were analysed by nonlinear regression to derive dissociation constants for the high- ($K_{i\text{-}high}$), and the low- ($K_{i\text{-}low}$) affinity states of the receptor. % High refers to the percentage of high-affinity binding sites as calculated from nonlinear fitting. Values are best fit ± S.E. of 3 experiments performed in duplicate. One-site model or two-site model as a better description of the data was determined by *F* test. Two-site model, $p < 0.001$. NA, two-site model not applicable ($p > 0.05$). DOM displacement curve of [^{3}H]ketanserin with 1 μM LY379 compared to DOM displacement curve of [^{3}H]ketanserin with vehicle: $F[5,155] = 12.24$, *$p < 0.001$. DOM displacement curve of [^{3}H]ketanserin with 10 μM LY379 compared to DOM displacement curve of [^{3}H]ketanserin with vehicle: $F[5,155] = 17.7$, **$p < 0.001$.

[^{3}H]Ketanserin binding displacement curves by DOB in mouse SCx membranes.

Ligand	$K_{i\text{-}high}$ (log M)	$K_{i\text{-}low}$ (log M)	% High
vehicle	-8.2 ± 0.2	-6.3 ± 0.08	33 ± 3
LY379 0.1μM	-9.0 ± 0.2*	-6.3 ± 0.07	30 ± 3
LY379 1μM	-9.0 ± 0.3**	-6.3 ± 0.11	33 ± 4
LY379 10μM	-9.3 ± 0.1***	-6.4 ± 0.07	33 ± 2
LY379 10μM + LY34	-8.1 ± 0.3	-6.4 ± 0.14	31 ± 7
GTPγS	NA	-6.1 ± 0.07	NA

DOB displacement of [^{3}H]ketanserin (2 nM; K_D = 2.72 nM) binding was performed in the absence (vehicle) or in the presence of LY379, LY34 (1 μM) or GTPγS (10 μM). Competition curves were analysed by nonlinear regression to derive dissociation constants for the high- ($K_{i\text{-}high}$), and the low- ($K_{i\text{-}low}$) affinity states of the receptor. % High refers to the percentage of high-affinity binding sites as calculated from nonlinear fitting. Values are best fit ± S.E. of 3 experiments performed in duplicate. One-site model or two-site model as a better description of the data was determined by *F* test. Two-site model, $p < 0.001$. NA, two-site model not applicable ($p > 0.05$).). DOB displacement curve of [^{3}H]ketanserin with 0.1 μM LY379 compared to DOB displacement curve of [^{3}H]ketanserin with vehicle: $F[5,142] = 4.57$, *$p < 0.001$. DOB displacement curve of [^{3}H]ketanserin with 1 μM LY379 compared to DOB displacement curve of [^{3}H]ketanserin with vehicle: $F[5,155] = 2.67$, **$p < 0.05$. DOB displacement curve of [^{3}H]ketanserin with 10 μM LY379 compared to DOB displacement curve of [^{3}H]ketanserin with vehicle: $F[5,155] = 11.39$, ***$p < 0.001$.

Supplementary Table S3

[^{3}H]LY341495 binding displacement curves by LY379 in mouse SCx membranes.

Ligand	$K_{i\text{-}high}$ (log M)	$K_{i\text{-}low}$ (log M)	% High
vehicle	-9.3 ± 0.2	-7.4 ± 0.04	19 ± 2
DOI 0.1μM	-9.4 ± 0.5	-7.5 ± 0.07	12 ± 4
DOI 1μM	NA	-7.6 ± 0.04	NA
DOI 10μM	NA	-7.6 ± 0.02	NA
DOI 10μM + ketanserin	-9.0 ± 0.3	-7.3 ± 0.06	18 ± 5
GTPγS	-8.6 ± 0.3	-7.3 ± 0.05	14 ± 5*

LY379 displacement of [^{3}H]LY341495 (2.5 nM; K_D = 2.11 nM) binding was performed in the absence (vehicle) or in the presence of DOI, ketanserin (1 μM) or GTPγS (10μM). Competition curves were analysed by nonlinear regression to derive dissociation constants for the high- ($K_{i\text{-}high}$), and the low- ($K_{i\text{-}low}$) affinity states of the receptor. % High refers to the percentage of high-affinity binding sites as calculated from nonlinear fitting. Values are best fit ± S.E. of 3-6 experiments performed in duplicate. One-site model or two-site model as a better description of the data was determined by *F* test. Two-site model, $p < 0.001$. NA, two-site model not applicable ($p > 0.05$). LY379 displacement curve of [^{3}H]LY341495 with GTPγS compared to LY379 displacement curve of [^{3}H]LY341495 with vehicle: $F[5,88] = 12.20$, *$p < 0.001$.

[^{3}H]LY341495 binding displacement curves by DCG-IV in mouse SCx membranes.

Ligand	$K_{i\text{-}high}$ (log M)	$K_{i\text{-}low}$ (log M)	% High
vehicle	-9.5 ± 0.2	-6.4 ± 0.04	14 ± 2
DOI 0.1μM	-9.1 ± 0.6	-6.4 ± 0.06	8 ± 3
DOI 1μM	NA	-6.2 ± 0.05	NA
DOI 10μM	NA	-6.3 ± 0.05	NA
DOI 10μM + ketanserin	-9.7 ± 0.6	-6.4 ± 0.07	12 ± 4
GTPγS	NA	-6.3 ± 0.06	NA

DCG-IV displacement of [^{3}H]LY341495 (2.5 nM; K_D = 2.11 nM) binding was performed in the absence (vehicle) or in the presence of DOI, ketanserin (1 μM) or GTPγS (10μM). Competition curves were analysed by nonlinear regression to derive dissociation constants for the high- ($K_{i\text{-}high}$), and the low- ($K_{i\text{-}low}$) affinity states of the receptor. % High refers to the percentage of high-affinity binding sites as calculated from nonlinear fitting. Values are best fit ± S.E. of 3 experiments performed in duplicate. One-site model or two-site model as a better description of the data was determined by *F* test. Two-site model, $p < 0.001$. NA, two-site model not applicable ($p > 0.05$).

[^{3}H]LY341495 binding displacement curves by L-CCG-I in mouse SCx membranes.

Ligand	$K_{i\text{-}high}$ (log M)	$K_{i\text{-}low}$ (log M)	% High
vehicle	NA	-6.0 ± 0.07	NA
DOI 0.1μM	NA	-5.8 ± 0.06	NA
DOI 1μM	NA	-5.1 ± 0.13*	NA
DOI 10μM	NA	-4.9 ± 0.08**	NA
DOI 10μM + ketanserin	NA	-6.0 ± 0.09	NA
GTPγS	NA	-5.1 ± 0.09***	NA

L-CCG-I displacement of [^{3}H]LY341495 (2.5 nM; K_D = 2.11 nM) binding was performed in the absence (vehicle) or in the presence of DOI, ketanserin (1 μM) or GTPγS (10μM). Competition curves were analysed by nonlinear regression to derive dissociation constants for the high- ($K_{i\text{-}high}$), and the low- ($K_{i\text{-}low}$) affinity states of the receptor. % High refers to the percentage of high-affinity binding sites as calculated from nonlinear fitting. Values are best fit ± S.E. of 3 experiments performed in duplicate. One-site model or two-site model as a better description of the data was determined by *F* test. Two-site model, $p < 0.001$. NA, two-site model not applicable ($p > 0.05$). L-CCG-I displacement curve of [^{3}H]LY341495 with 1 μM DOI compared to L-CCG-I displacement curve of [^{3}H]LY341495 with vehicle: $F[3,78] = 56.49$, *$p < 0.001$. L-CCG-I displacement curve of [^{3}H]LY341495 with 10 μM DOI compared to L-CCG-I displacement curve of [^{3}H]LY341495 with vehicle: $F[3,78] = 51.82$, **$p < 0.001$. L-CCG-I displacement curve of [^{3}H]LY341495 with GTPγS compared to L-CCG-I displacement curve of [^{3}H]LY341495 with vehicle: $F[3,64] = 24.34$, **$p < 0.001$.

Supplementary S4. [^{3}H]Ketanserin binding displacement curves by DOI in HEK293 cell membranes stably expressing 2AR.

mGluR	Ligand	$K_{i\text{-}high}$ (log M)	$K_{i\text{-}low}$ (log M)	% High
mock	vehicle	-8.9 ± 0.2	-7.1 ± 0.2	35 ± 9
mock	GTP□S	NA	-6.7 ± 0.0	NA
mGluR2 (646 fmol/mg prot)	vehicle	-9.1 ± 0.3	-7.1 ± 0.1	30 ± 8
mGluR2 (1343 fmol/mg prot)	vehicle	-9.1 ± 0.4	-7.1 ± 0.2	28 ± 3
mGluR2 (1994 fmol/mg prot)	vehicle	NA	-7.7 ± 0.1	NA
mGluR2 (2800 fmol/mg prot)	vehicle	NA	-7.1 ± 0.0	NA
mGluR2 (3587 fmol/mg prot)	vehicle	NA	-7.4 ± 0.0	NA
mGluR2 (3587 fmol/mg prot)	LY379	-9.5 ± 0.1	-7.4 ± 0.1	28 ± 5
mGluR3 (4185 fmol/mg prot)	vehicle	-9.3 ± 0.2	-7.2 ± 0.1	29 ± 4
mGluR3 (4185 fmol/mg prot)	LY379	-9.3 ± 0.4	-7.3 ± 0.1	25 ± 5

DOI displacement of [^{3}H]ketanserin (2 nM; K_D = 0.37 nM) binding was performed in HEK293 cells stably expressing 2AR (504 ± 25 fmol/mg prot) and transfected with mock, mGluR2 or mGluR3 in the absence (vehicle) or in the presence of LY379 (10 μM). HEK293 cells were expressing different densities of mGluR2 or mGluR3 (see Supplementary Fig. S4). Competition curves were analysed by nonlinear regression to derive dissociation constants for the high- ($K_{i\text{-}high}$), and the low- ($K_{i\text{-}low}$) affinity states of the receptor. % High refers to the percentage of high-affinity binding sites as calculated from nonlinear fitting. Values are best fit ± S.E. of three experiments performed in triplicate. One-site model or two-site model as a better description of the data was determined by F test. Two-site model, $p < 0.001$. NA, two-site model not applicable ($p > 0.05$).

Supplementary Table S5. [^{3}H]Ketanserin binding displacement curves by DOI in HEK293 cell membranes stably expressing 2AR.

mGluR	$K_{i\text{-}high}$ (log M)	$K_{i\text{-}low}$ (log M)	% High
mock	-9.2 ± 0.3	-7.2 ± 0.1	30 ± 7
mGluR2	NA	-7.2 ± 0.0	NA
mGluR3	-9.3 ± 0.2	-7.4 ± 0.1	24 ± 7
□mGluR2	NA	-7.5 ± 0.1	NA
mGluR2□TM4,5	-9.2 ± 0.2	-6.9 ± 0.2	33 ± 9
mGluR3□TM1-5	NA	-7.4 ± 0.0	NA
mGluR3□TM4,5	NA	-7.3 ± 0.0	NA

DOI displacement of [^{3}H]ketanserin (2 nM; K_D = 0.37 nM) binding was performed in HEK293 cells stably expressing 2AR (504 ± 25 fmol/mg prot) and transfected with mock, mGluR2, mGluR3 or mGluR2/mGluR3 chimeras (See Supplementary Fig. S5). Competition curves were analysed by nonlinear regression to derive dissociation constants for the high- ($K_{i\text{-}high}$), and the low- ($K_{i\text{-}low}$) affinity states of the receptor. % High refers to the percentage of high-affinity binding sites as calculated from nonlinear fitting. Values are best fit ± S.E. of three experiments performed in triplicate. One-site model or two-site model as a better description of the data was determined by F test. Two-site model, $p < 0.001$. NA, two-site model not applicable ($p > 0.05$).

Supplementary Table S6. DOI-stimulated [^{35}S]GTPγS binding followed by immunoprecipitation with anti-G$\alpha_{q/11}$ antibody in HEK293 cell membranes stably expressing 2AR.

mGluR	Ligand	E_{max}	$EC_{50\text{-}high}$ (log M)	log $EC_{50\text{-}low}$ (log M)	% High
mock	vehicle	212 ± 19	-8.4 ± 0.7	-5.1 ± 0.4	39 ± 12
mGluR2	vehicle	221 ± 12	NA	-6.1 ± 0.2	NA
mGluR2	LY379	218 ± 10	-7.6 ± 0.3	-5.0 ± 0.1	40 ± 7
mGluR3	vehicle	215 ± 8	-8.4 ± 0.2	-5.0 ± 0.1	38 ± 4
mGluR3□TM4,5	vehicle	225 ± 10	NA	-5.9 ± 0.1	NA

[^{35}S]GTPγS binding followed by immunoprecipitation with anti-G$\alpha_{q/11}$ antibody in HEK293 cells stably expressing 2AR and transfected with mock, mGluR2, mGluR2 or mGluR3□TM4,5. [^{35}S]GTPγS binding was performed in the presence or in the absence of LY379 (10 μM). Concentration-response curves were analysed by nonlinear regression to derive constants for efficacy (E_{max}, % over basal [^{35}S]GTPγS binding) and high- ($EC_{50\text{-}high}$) and low- ($EC_{50\text{-}low}$) potencies for DOI. % High refers to the percentage of high-potency binding sites as calculated from nonlinear fitting. Basal binding for nonlinear regression was the [^{35}S]GTPγS binding to G$\alpha_{q/11}$ protein in the absence of DOI for each experimental condition. Values are best fit ± S.E. of three experiments performed in duplicate. Monophasic model or biphasic concentration-response model as a better description of the data was determined by F test. Biphasic model, $p < 0.05$, $p < 0.001$, and $p < 0.001$ for mock/vehicle, mGluR2/LY379 and mGluR3/vehicle curves, respectively. NA, biphasic model not applicable ($p > 0.05$). DOI activating G$\alpha_{q/11}$ in cortical primary cultures (see Fig. 3a): pEC_{50} vehicle, -6.7±0.1; $pEC_{50\text{-}high}$ LY379, -7.6±0.4; and $pEC_{50\text{-}low}$ LY379, -5.0±0.3 ($F[3,57] = 4.61$, $p < 0.01$).

Supplementary Table S7. DOI-stimulated [^{35}S]GTPγS binding followed by immunoprecipitation with anti-G$\alpha_{i1,2,3}$ antibody in HEK293 cell membranes stably expressing 2AR.

mGluR2	Ligand	E_{max}	log $EC_{50\text{-}high}$	log $EC_{50\text{-}low}$	% High
mock	vehicle	16.8 ± 2	NA	-4.8 ± 0.3	NA
mGluR2	vehicle	22.8 ± 1**	NA	-6.9 ± 0.2*	NA
mGluR2	LY379	11.9 ± 1	NA	-4.9 ± 0.3	NA
mGluR3	vehicle	14.07 ± 1	NA	-4.6 ± 0.3	NA
mGluR3□TM4,5	vehicle	24.73 ± 1***	NA	-6.4 ± 0.3***	NA

[^{35}S]GTPγS binding followed by immunoprecipitation with anti-G$\alpha_{i1,2,3}$ antibody in HEK293 cells stably expressing 2AR and transfected with mock, mGluR2, mGluR2 or mGluR3□TM4,5. [^{35}S]GTPγS binding was performed in the presence or in the absence of LY379 (10 μM). Concentration-response curves were analysed by nonlinear regression to derive constants for efficacy (E_{max}, % over basal [^{35}S]GTPγS binding) and high- ($EC_{50\text{-}high}$) and low- ($EC_{50\text{-}low}$) potencies for DOI. % High refers to the percentage of high-potency binding sites as calculated from nonlinear fitting. Basal binding for nonlinear regression was the [^{35}S]GTPγS binding to G$\alpha_{i1/2/3}$ protein in the absence of DOI for each experimental condition. Values are best fit ± S.E. of three experiments performed in duplicate. Monophasic concentration-response model provided a better description of the data as determined by F test. NA, biphasic model not applicable ($p > 0.05$). DOI concentration-response curve with mGluR2/vehicle compared to DOI concentration-response curve with mock/vehicle: $F[3,90] = 19.57$, *$p < 0.001$. DOI concentration-response curve with mGluR2/vehicle compared to DOI-concentration response curve with mGluR2/LY379: $F[3,91] = 30.70$, ** $p < 0.001$. DOI concentration-response curve with mGluR2/vehicle compared to DOI-concentration response curve with mGluR3□TM4,5/vehicle: $F[3,75] = 6.25$, *** $p < 0.001$. DOI activating G$\alpha_{i1,2,3}$ in cortical primary cultures (see Fig. 3a): pEC_{50} vehicle, -6.1±0.1; pEC_{50} LY379, -4.3±0.2 ($F[3,84] = 50.82$, $p < 0.001$).

Supplementary Table S8. Demographic characteristics and antemortem diagnoses of cases of nontreated schizophrenic subjects, and their respective control subjects.

	Gender (F/M)	Age at death (years)	Postmortem delay (h)	Antipsychotic treatment	Additional drugs
Schizophrenic 1	M	41	41	Untreated	BDZ
Control 1	M	41	24		
Schizophrenic 2	M	49	41	Untreated	
Control 2	M	49	17		
Schizophrenic 3	M	24	45	Untreated	
Control 3	M	25	42		
Schizophrenic 4	M	44	31	Untreated	BDZ; CBZ
Control 4	M	45	30		
Schizophrenic 5	F	39	11	Untreated	
Control 5	F	35	8		
Schizophrenic 6	M	43	19	Untreated	
Control 6	M	48	16		
Schizophrenic 7	M	21	24	Untreated	
Control 7	M	21	16		
Schizophrenic 8	M	23	43	Untreated	
Control 8	M	23	27		
Schizophrenic 9	M	33	36	Untreated	BDZ
Control 9	M	33	41		
Schizophrenic 10	M	31	14	Untreated	BDZ
Control 10	M	31	59		
Schizophrenic 11	M	41	16	Untreated	
Control 11	M	40	12		
Schizophrenic 12	F	25	19	Untreated	
Control 12	F	30	15		
Schizophrenic 13	M	30	13	Untreated	CC
Control 13	M	27	10		
Schizophrenia group	2F/11M	34 ± 3	27 ± 4		
Control group	2F/11M	34 ± 3	24 ± 4		

Antipsychotics were not detected in blood samples of schizophrenics. All schizophrenic subjects included, except schizophrenic 5 and schizophrenic 6, committed suicide. Abbreviations: benzodiazepines (BDZ), carbamazepine (CBZ), and cocaine (CC).

Supplementary Table S9. Demographic characteristics and antemortem diagnoses of cases of antipsychotic-treated schizophrenic subjects, and their respective control subjects.

	Gender (F/M)	Age at death (years)	Postmortem delay (h)	Antipsychotic treatment	Additional drugs
Schizophrenic 14	M	66	57	OLA	
Control 14	M	66	50		
Schizophrenic 15	F	30	17	HAL	BDZ; TRA
Control 15	F	29	31		
Schizophrenic 16	M	57	19	QUE	
Control 16	M	58	19		ETH (0.99 g/l)
Schizophrenic 17	M	56	8	QUE	BDZ
Control 17	M	55	15		
Schizophrenic 18	M	37	11	OLA	BDZ
Control 18	M	36	14		ETH (0.3 g/l)
Schizophrenic 19	F	35	3	QUE	BDZ
Control 19	F	35	22		
Schizophrenic 20	F	56	13	CLZ	FUR
Control 20	F	52	64		
Schizophrenic 21	M	44	6	CLT; LEV	BIP; BDZ
Control 21	M	42	9		
Schizophrenic 22	M	30	18	OLA	
Control 22	M	30	11		
Schizophrenic 23	M	32	8	QUE	BDZ; PAR
Control 23	M	32	27		AMP; ETH (0.68 g/l)
Schizophrenic 24	M	27	17	CLZ	
Control 24	M	30	10		
Schizophrenic 25	M	43	65	CLZ	
Control 25	M	38	59		
Schizophrenia group	3F/9M	43 ± 4	20 ± 6		
Control group	3F/9M	42 ± 4	28 ± 6		

Therapeutic levels of olanzapine (OLA), haloperidol (HAL), quetiapine (QUE), clozapine (CLZ), clotiapine (CLT), and levomepromazine (LEV) were detected in blood samples of schizophrenics. All schizophrenic subjects included, except schizophrenic 21 and schizophrenic 25, committed suicide. Abbreviations: benzodiazepines (BDZ), trazodone (TRA), furosemide (FUR), biperiden (BIP), amphetamine (AMP), and paracetamol (PAR). Ethanol in blood is coded as ETH.

Supplementary Table S10. Oligonucleotide probe sequences for FISH

htr2A
ATCCCTGGAGTTGAAGTCATTAGGGTAGAGCCTCGAGTCGTCACCTAATT
TTCTGTTCTCCTTGTACTGGCACTGAATGTACCGTGAGAAGGCGGACCTA
TTTCCACATCAGAAATTCTCGCGGCAATGACGGCATTCTAGCCAAGCGTG
CCTCGCTTCACAGTGCTAGGGAGAGTCCACGGCGGAGCTGTAAGTTCTCA
CCAGTGGGTTGACGGCTGAGGAGAGATAACCAATCCAGACAAACACATTG
grm2
CATGGGATGATGCTAGTATCCAGAGTCAGACCTTCTGCCCAGTAGCCTAA
ACAGTCAGCACAGGTGAACTCATCCAGCCTGTACTCATAGGGCTGACAGG
GGTCTTGAAGGCATAGAGCGTGCAGAGAGCGATGAGGAGCACGTTGTAGG
ACATCGTAGTGGTCTGCACCCGATAATCACTGGAGGTGACGTAGAAGATG
GCTCACCACGTTCTTCTGTGGCTGGAAGAGGATAATGTGCAGCTTGGGTG
grm3
TTTGGCACTGGTGGAGGCGTAGCTTATCTGAGGGATCTGGAAGAGCCTCA
CTGTCTCCCCATAGTCACCTTCAGAGGCAACAGTGGACACATAGGTCCAG
ACAAATCTGTCTGTGGTTTCTCTTGTTCTGGAGGCTGCACTGGAACTTCT
GTACAACTTCTTTCCATCCAGGATCTTCATTGCATCACAGAGCTTGGTGG
TCATTTCATTGGGGGCACAGGGATCACTGCACTGGGAAGTGGGGACTGAG
c-fos
TCCTCTTCAGGAGATAGCTGCTCTACTTTGCCCCTTCTGCCGATGCTCTG
CTTCAAGTTGATCTGTCTCCGCTTGGAGTGTATCTGTCAGCTCCCTCCTC
TCCTCAGACTCTGGGGTGGAAGCCTCAGGCAGACCTCCAGTCAAATCCAG
GATGCCGGAAACAAGAAGTCATCAAAGGGTTCTGCCTTCAGCTCCACGTT
egr-2
TCTCCAGTCATGTCAATGTTGATCATGCCATCTCCCGCCACTCCGTTCAT
TGGATCTCTCTGGCACGGAGATGGAAAAAATCCAGGATAGTCTGGGATCA
CTGGTCAGCTCATCAGAGCGTGAGAACCTCCTATCACAACCTTCTGCTGG
TCAGAACAACTGGCATCCAGGGTCAACGGAAAGGGCTAGCAGACCATAGT
Scrambled
TTCACGGGCCTCTTGAAGTTGCTCCGGTTCAAGTAGCCGAAATGGTACAT
GTGGAGTTGTCCAAGTCACAGTCACCTTGACGCTGGTGTATAAGAGTCAG
TACTTGCCTCACCGCCCTCTACCGTACTAGTTGTAACTGTACTGACCTCT
TCCTCGTCTGTCGTAACACTTCAAACTGTGAATGCCTCTGCCCTACCCTT
GTGGGTTCGACGTGTAATAGGAGAAGGTCGGTGTCTTCTTGCACCACTCG

Boldface letters represent amino-modified nucleotides, which were labeled with succinimidyl esters Alexa fluorophores.

Supplementary Table S11. Mouse qRT-PCR prime pairs

Gene Name	GenBank	Primer pairs	
		Forward	Reverse
grm1	NM_016976	AAGGGACAGCATGTGTGGCA	ACTCTTGCCAGAGCCTTGGT
grm2	XM_909627	CCATCTTCTACGTCACCTCC	AGGAACAAGCTGGGATCCAG
grm3	NM_181850	TGACTACAGAGTGCAGACGAC	TCGCAGTTCCACTGACACTG
grm4	NM_00101338	ATTGCTGCCACGCTGTTCGT	AGGAAGGTGGTGGCATAGCA
grm5	NM_00108141	AGCTGTGCACACAGAAGGCA	AGTGGGCGATGCAAATCCCT
grm6	NM_173372	ATCTTCTTTGGCACCGCCCA	TCTGCACGTTCTGCTCTGGA
grm7	NM_177328	TTGGCACAGCGCAATCAGCA	TGCTGTGACTACGGCCTTGA
grm8	NM_008174	ATGATTGCGGCACCTGACAC	TGGGATGCTGGGCTGATGAA
c-fos	J00370	TTCCTGGCAATAGCGTGTTC	TTCAGACCACCTCGACAATG
egr-2	NM_000399	TGTTAACAGGGTCTGCATGTG	AGCGGCAGTGACATTGAAG
□-actin	X03672	AGGTGACAGCATTGCTTCTG	GCTGCCTCAACACCTCAAC
GAPDH	NM_008084	TGCGACTTCAACAGCAACTC	CTTGCTCAGTGTCCTTGCTG
mapkapk5	NM_010765	CATTGCCCAGTGTATCCTCC	ACCTGCTTTACCACCTCTGC
rpS3	NM_012052	AGGTTGTGGTGTCTGGGAAG	GAGGCTTCTTGGGACCAATC

Supplementary Table S12. Human qRT-PCR prime pairs

Gene Name	GenBank	Primer pairs	
		Forward	Reverse
grm2	NM_000839	GCACAGGCAAGGAGACAGC	GAGGCAGCCAAGCACCAC
grm3	NM_000840	TCCACCCCTCCGTTTTCCC	TCATGCTAGTCCTCTCTCATTTCC
β-actin	NM_001101	GGAAATCGTGCGTGACATTAAGG	GATGGAGGGGCCGGACTC

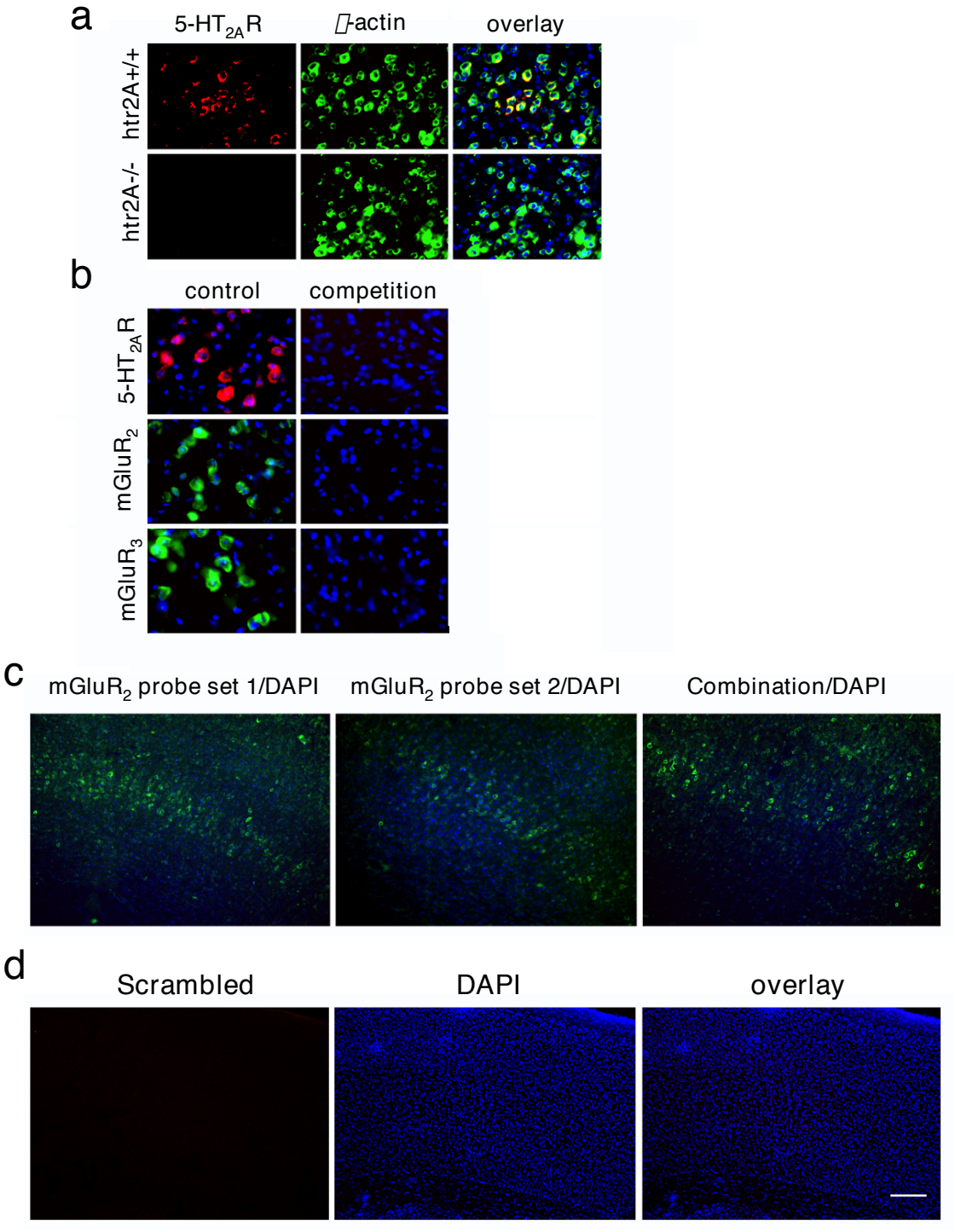

Supplementary Fig. S1

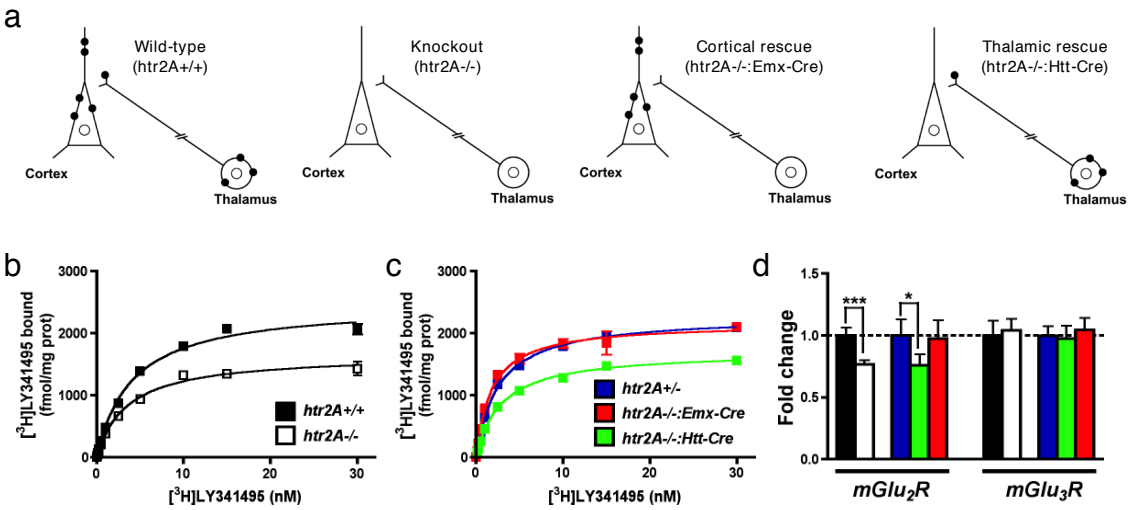

Supplementary Fig. S2

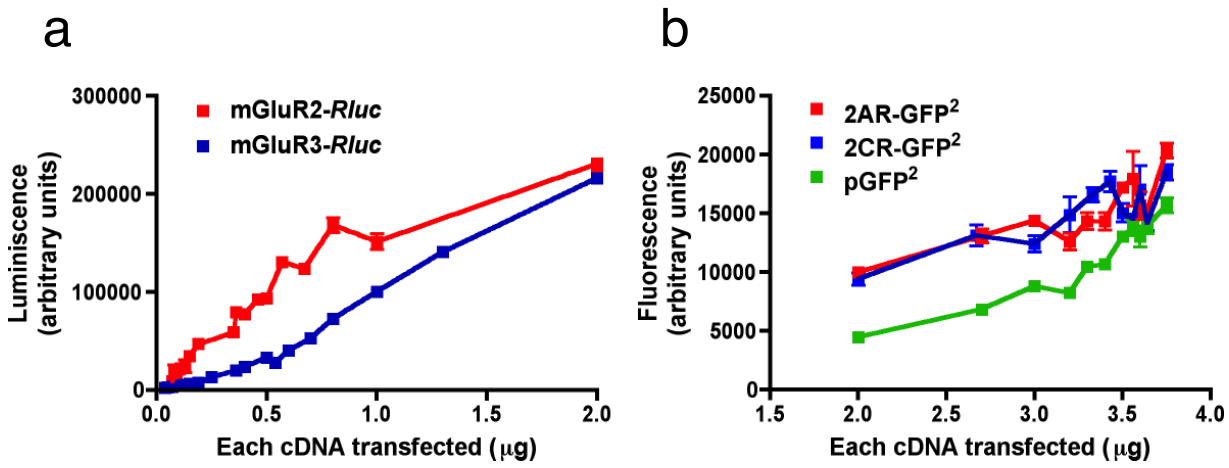

Supplementary Fig. S3

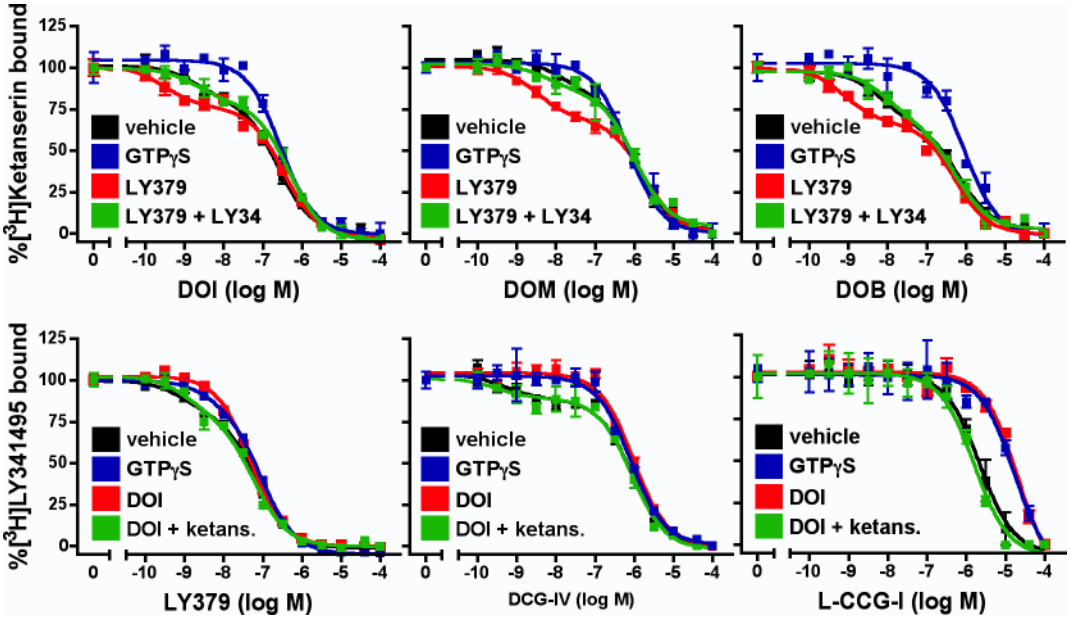

Supplementary Fig. S4

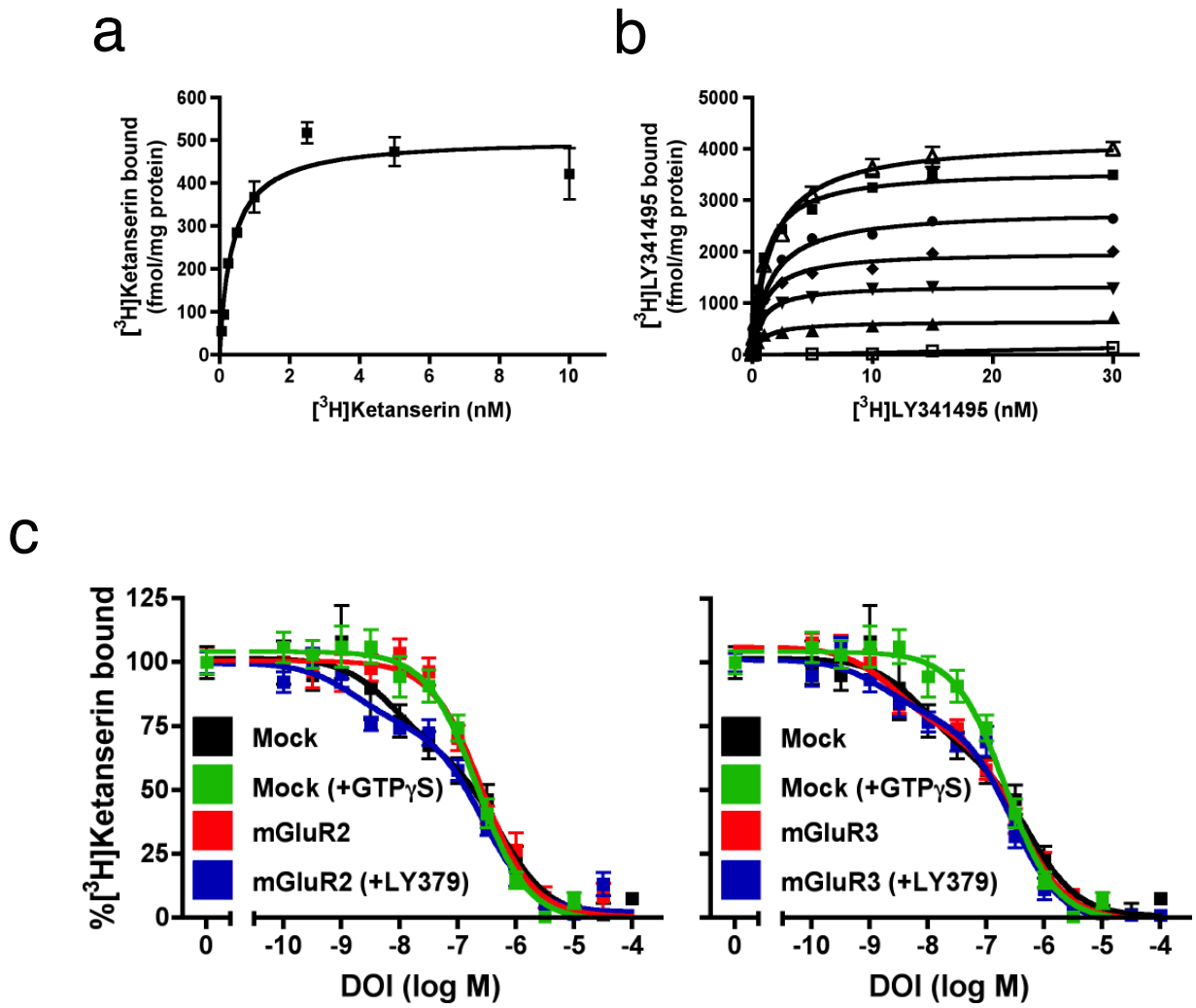

Supplementary Fig. S5

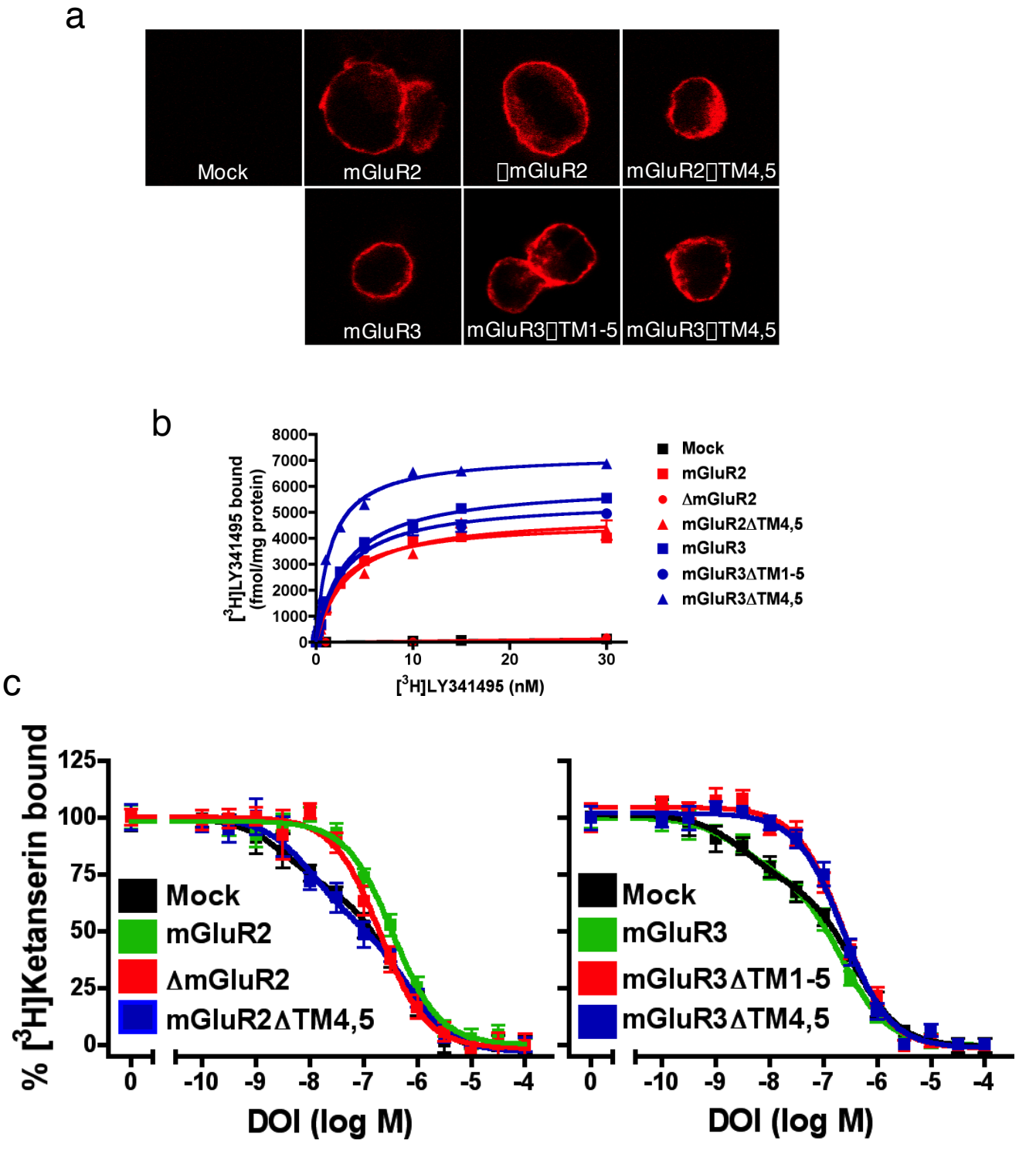

Supplementary Fig. S6

TM1	1.30	
MGR2_HUMAN	562	RWGDAWAVGPVTIACLGALATLFVLGVFVR
MGR2_RAT	562	RWGDAWAVGPVTIACLGALATLFVLGVFVR
MGR3_HUMAN	571	RWEDAWAIGPVTIACLGFMCTCMVVTVFIK
MGR3_PONPY	571	RWEDAWVIGPVTIACLGFMCTCMVVTVFIK
MGR3_MOUSE	571	RWEDAWAIGPVTIACLGFMCTCIVITVFIK
MGR3_RAT	571	KWEDAWAIGPVTIACLGFLCTCIVITVFIK
5HT2A_HUMAN	72	QEKNWSALLTAVVIILTIAGNILVIMAVSL
B2AR_HUMAN	31	VWVVGMGIVMSLIVLAIVFGNVLVITAIAK
OPSD_BOVIN	35	WQFSMLAAYMFLLIMLGFPINFLTLYVTVQ
TM2	2.38	
MGR2_HUMAN	600	ASGRELCYILLGGVFLCYCMTFIFIAK
MGR2_RAT	600	ASGRELCYILLGGVFLCYCMTFVFIAK
MGR3_HUMAN	609	ASGRELCYILLFGVGLSYCMTFFFIAK
MGR3_PONPY	609	ASGRELCYILLFGVGLSYCMTFFFIAK
MGR3_MOUSE	609	ASGRELCYILLFGVSLSYCMTFFFIAK
MGR3_RAT	609	ASGRELCYILLFGVSLSYCMTFFFIAK
5HT2A_HUMAN	108	ATNYFLMSLAIADMLLGFLVMPVSMLT
B2AR_HUMAN	67	VTNYFITSLACADLVMGLAVVPFGAAH
OPSD_BOVIN	71	PLNYILLNLAVADLFMVFGGFTTTLYT
TM3	3.22	
MGR2_HUMAN	629	TAVCTLRRLGLGTAFSVCYSALLTKTNRIARIF
MGR2_RAT	629	TAVCTLRRLGLGTAFSVCYSALLTKTNRIARIF
MGR3_HUMAN	638	PVICALRRLGLGSSFAICYSALLTKTNCIARIF
MGR3_PONPY	638	PVICALRRLGLGTSFAICYSALLTKTNCIARIF
MGR3_RAT	638	PVICALRRLGLGTSFAICYSALLTKTNCIARIF
5HT2A_HUMAN	145	SKLCAVWIYLDVLFSTASIMHLCAISLDRYVAI
B2AR_HUMAN	103	NFWCEFWTSIDVLCVTASIETLCVIAVDRYFAI
OPSD_BOVIN	107	PTGCNLEGFFATLGGEIALWSLVVLAIERYVVV
TM4	4.40	
MGR2_HUMAN	677	ASQVAICLALISGQLLIVVAWLV
MGR2_RAT	677	ASQVAICLALISGQLLIVAAWLV
MGR3_HUMAN	686	SSQVFICLGLILVQIVMVSVWLI
MGR3_PONPY	686	SSQVFICLGLILVQIVMVSVWLI
MGR3_MOUSE	686	SSQVFICLGLILVQIVMVSVWLI
MGR3_RAT	686	SSQVFICLGLILVQIVMVSVWLI
5HT2A_HUMAN	190	TKAFLKIIAVWTISVGISMPIPV
B2AR_HUMAN	148	NKARVIILMVWIVSGLTSFLPIQ
OPSD_BOVIN	151	NHAIMGVAFTWVMALACAAPPLV
TM5	5.38	
MGR2_HUMAN	726	ASMLGSLAYNVLLIALCTLYAFK
MGR2_RAT	726	ASMLGSLAYNVLLIALCTLYAFK
MGR3_HUMAN	735	SSMLISLTYDVILVILCTVYAFK
MGR3_PONPY	735	SSMLISLTYDVILVILCTVYAFK
MGR3_MOUSE	735	SSMLISLTYDVVLVILCTVYAFK
MGR3_RAT	735	SSMLISLTYDVVLVILCTVYAFK
5HT2A_HUMAN	234	FVLIGSFVSFFIPLTIMVITYFL
B2AR_HUMAN	199	YAIASSIVSFYVPLVIMVFVYSR
OPSD_BOVIN	203	FVIYMFVVHFIIPLIVIFFCYGQ
TM6	6.32	
MGR2_HUMAN	757	NEAKFIGFTMYTTCIIWLAFLPIFYVTSS
MGR2_RAT	757	NEAKFIGFTMYTTCIIWLAFLPIFYVTSS
MGR3_HUMAN	766	NEAKFIGFTMYTTCIIWLAFLPIFYVTSS
MGR3_PONPY	766	NEAKFIGFTMYTTCIIWLAFLPIFYVTSS
MGR3_MOUSE	766	NEAKFIGFTMYTTCIIWLAFLPIFYVTSS
MGR3_RAT	766	NEAKFIGFTMYTTCIIWLAFLPIFYVTSS
5HT2A_HUMAN	320	KACKVLGIVFFLFVVMWCPFFITNIMAVI
B2AR_HUMAN	270	KALKTLGIIMGTFTLCWLPFFIVNIVHVI
OPSD_BOVIN	249	EVTRMVIIMVIAFLICWLPYAGVAFYIFT
TM7	7.33	
MGR2_HUMAN	788	RVQTTTMCVSVSLSGSVVLGCLFAPKLHIILFQPQKNV
MGR2_RAT	788	RVQTTTMCVSVSLSGSVVLGCLFAPKLHIILFQPQKNV
MGR3_HUMAN	797	RVQTTTMCISVSLSGFVVLGCLFAPKVHIILFQPQKNV
MGR3_PONPY	797	RVQTTTMCISVSLSGFVVLGCLFAPKVHIILFQPQKNV
MGR3_MOUSE	797	RVQTTTMCISVSLSGFVVLGCLFAPKVHIVLFQPQKNV
MGR3_RAT	797	RVQTTTMCISVSLSGFVVLGCLFAPKVHIVLFQPQKNV
5HT2A_HUMAN	360	ALLNVFVWIGYLSSAVNPLVYTLFNKTYRSAFSRYIQC
B2AR_HUMAN	306	EVYILLNWIGYVNSGFNPLIYCR-SPDFRIAFQELLCL
OPSD_BOVIN	286	IFMTIPAFFAKTSAVYNPVIYIMMNKQFRNCMVTTLCC

Supplementary Fig. S7

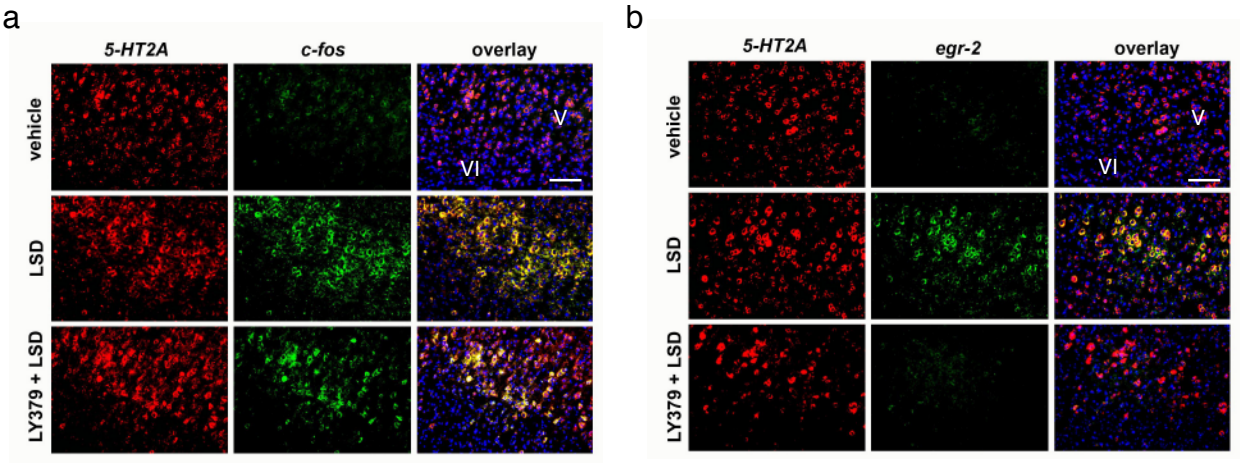

Supplementary Fig. S8

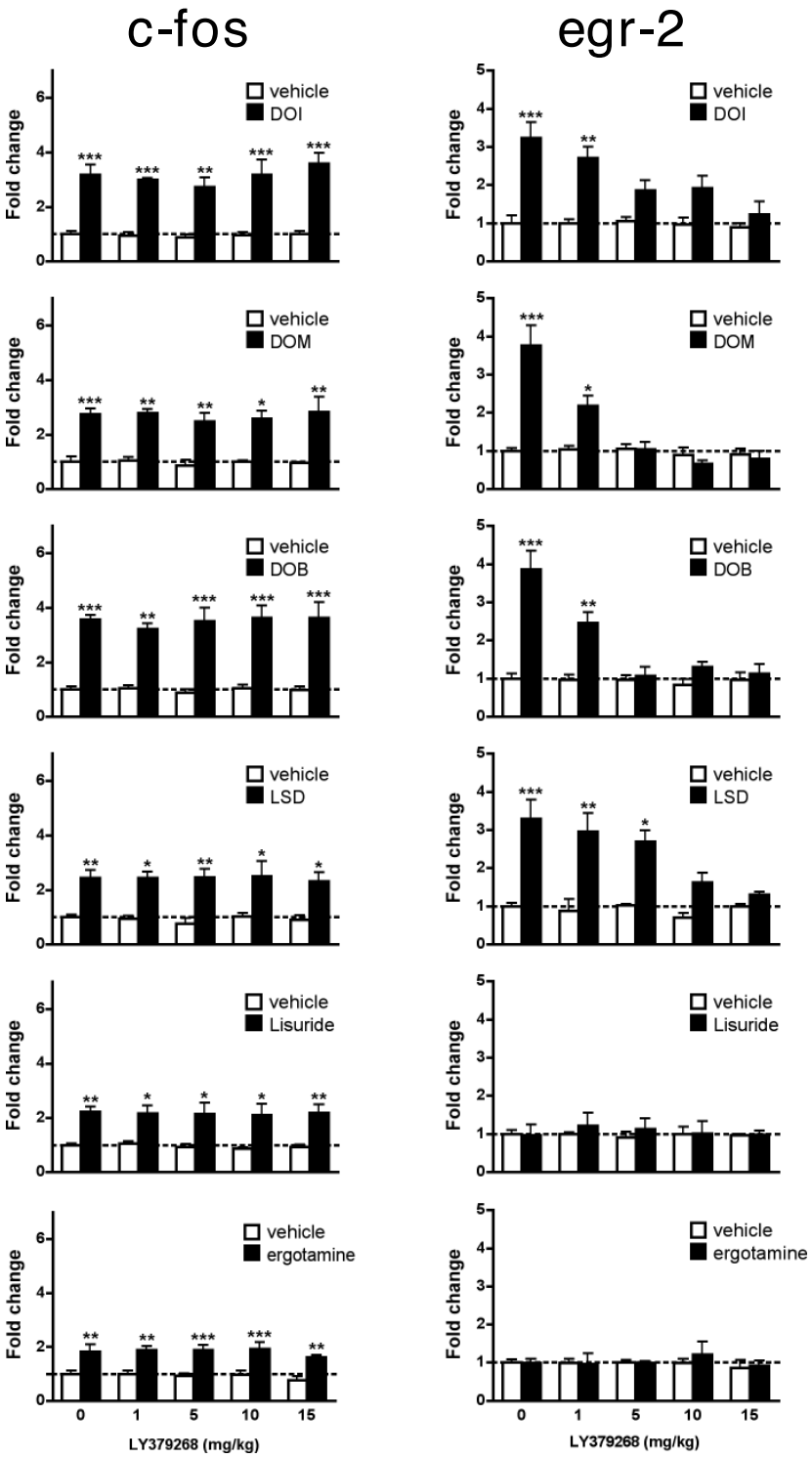

Supplementary Fig. S9

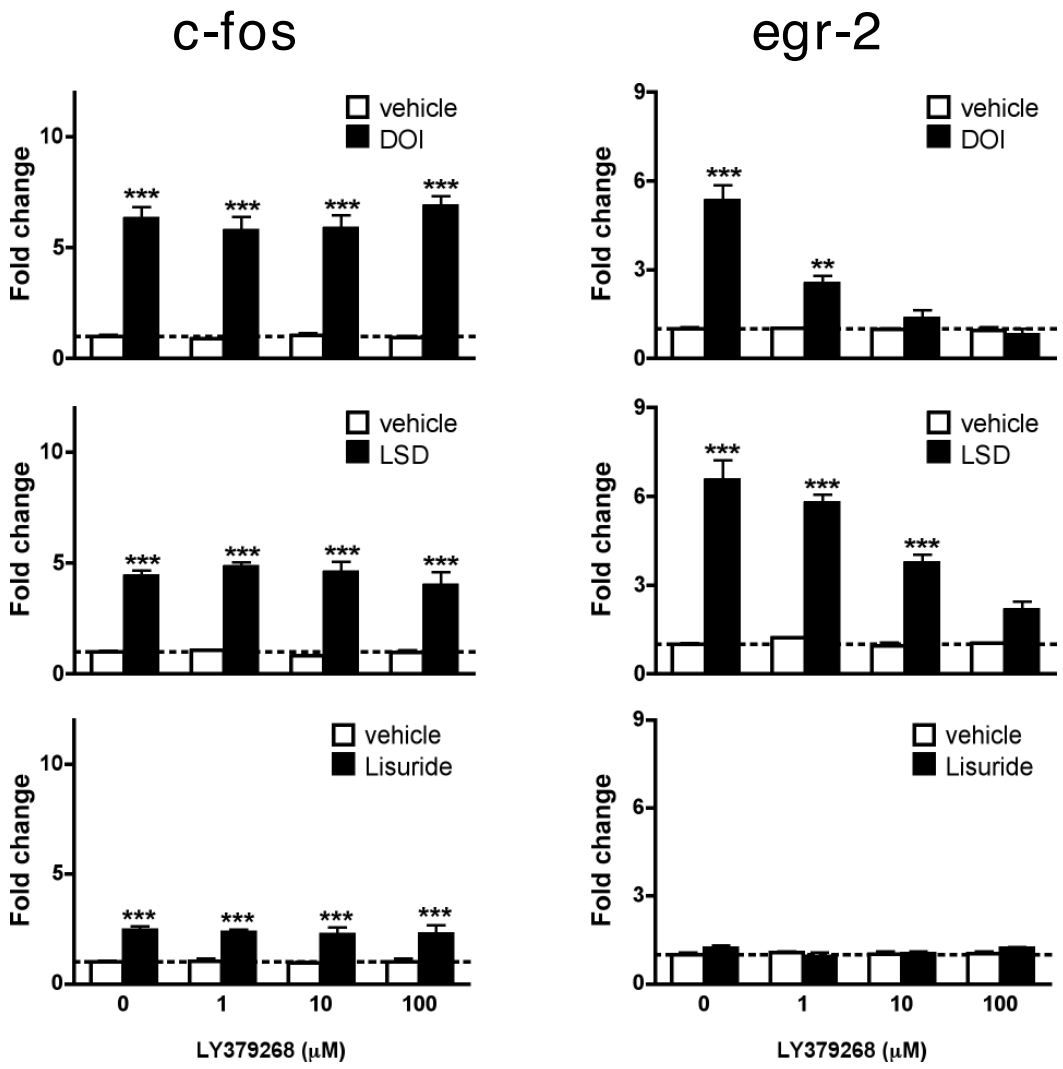

Supplementary Fig. 10

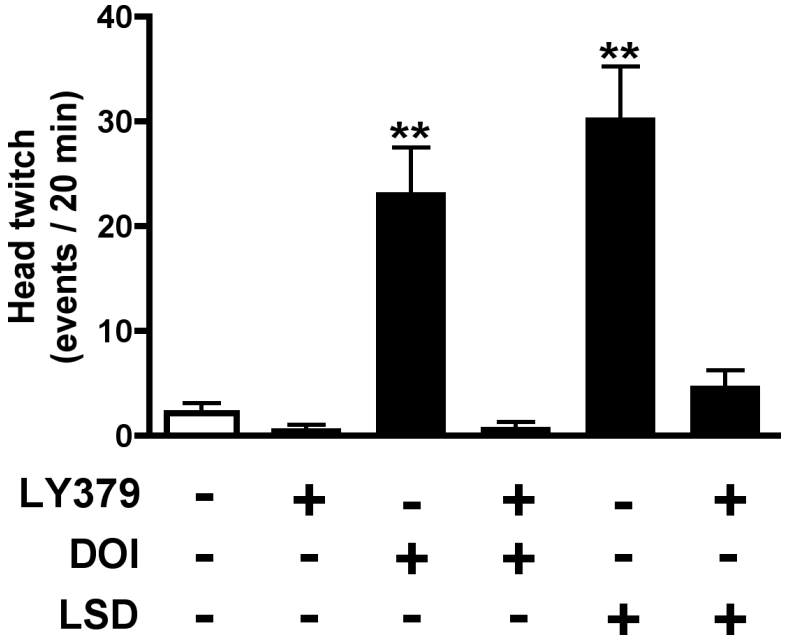

Supplementary Fig. S11

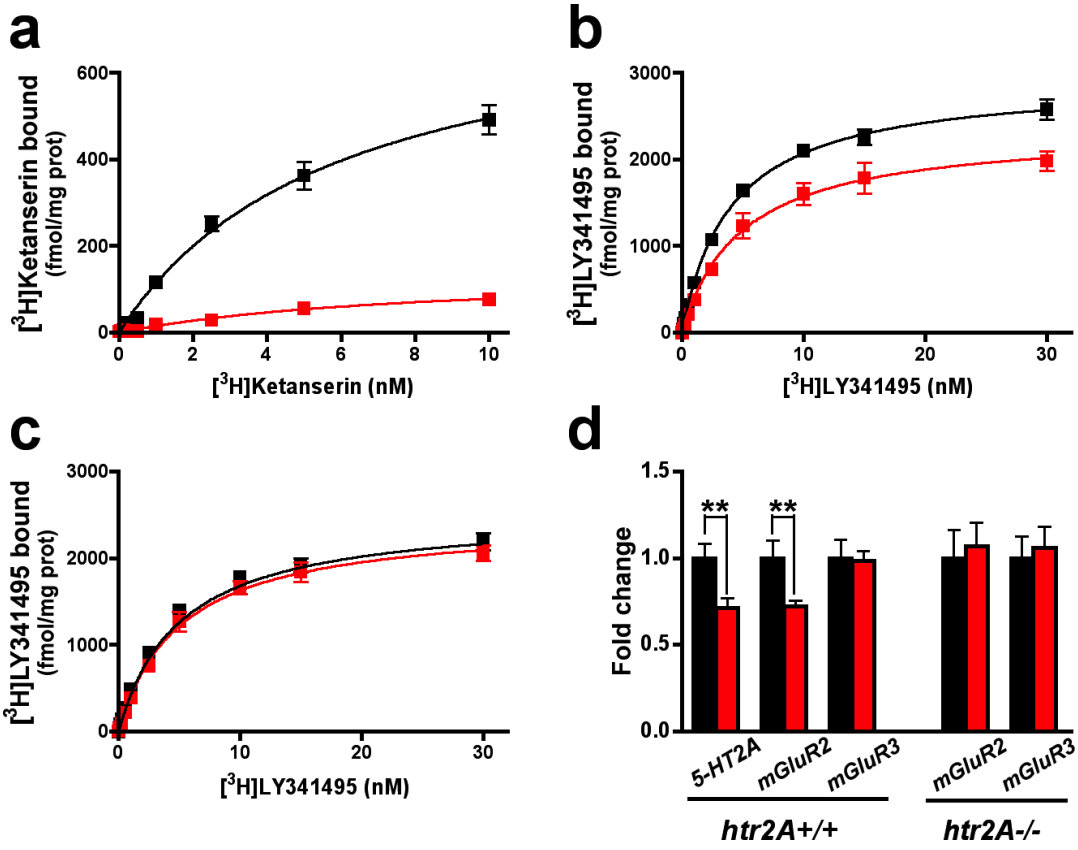

Supplementary Fig. S12

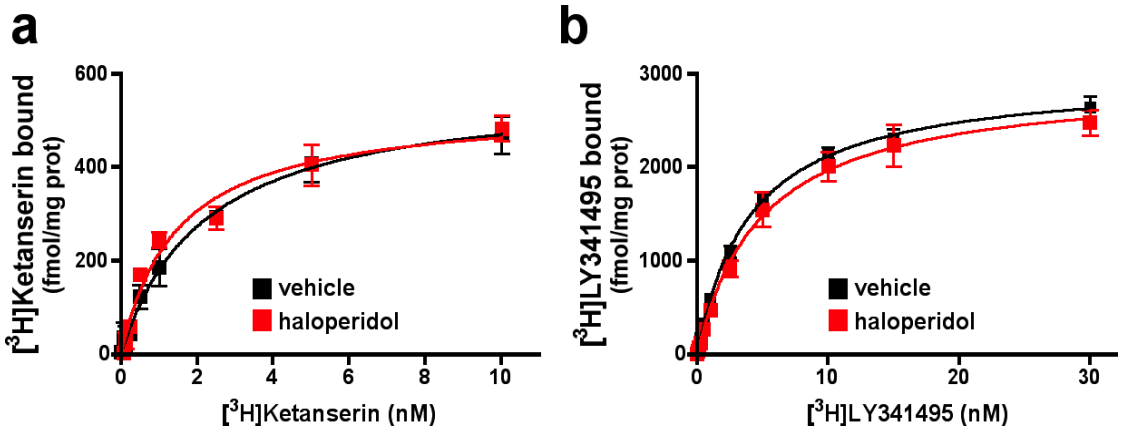

Supplementary Fig. 13

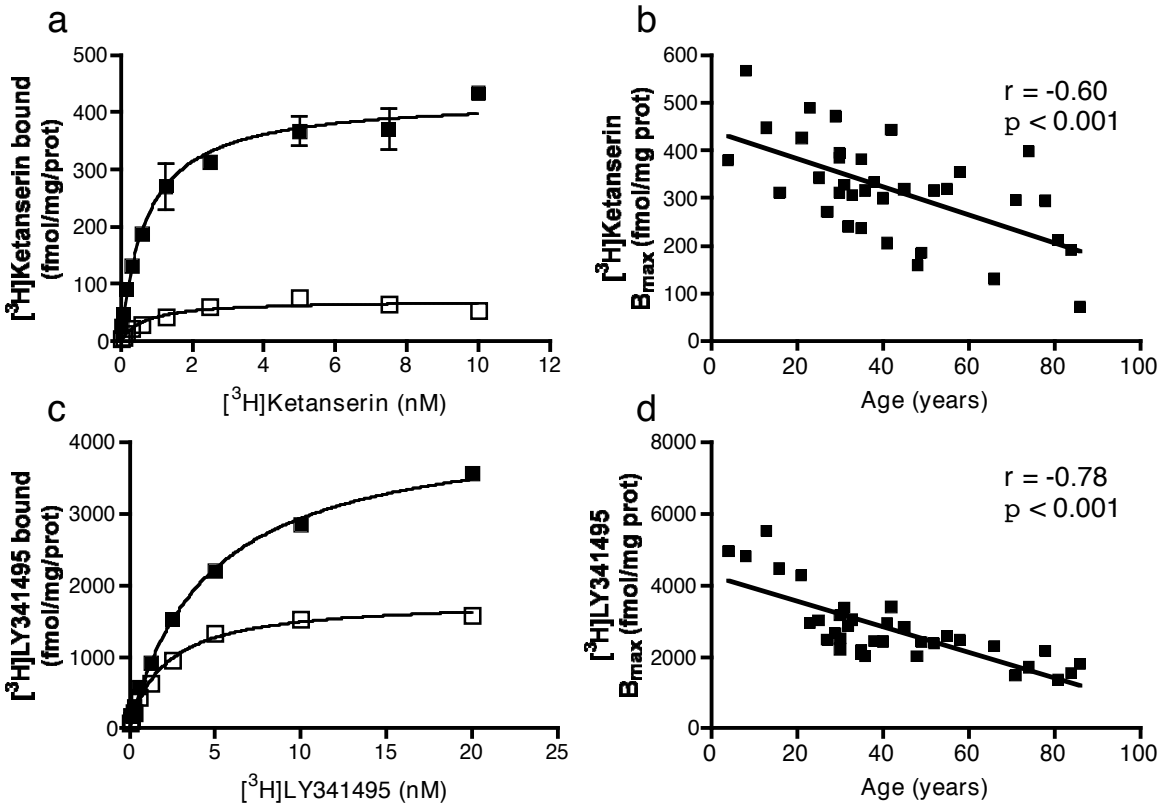

Supplementary Fig. S14